

Technical University Munich
Physics Department

Max Planck Institute for Physics
Werner Heisenberg Institute



Master's Thesis

Analysis of First Tritium Data of the KATRIN Experiment

Author:
Christian Karl

Supervisor:
Prof. Dr. Susanne Mertens

9th October 2018

Declaration of Authorship

English:

I hereby declare that I have written the present Master's thesis in the course Nuclear, Particle and Astrophysics independently only using the cited external resources.

German:

Ich erkläre hiermit, dass ich die vorliegende Abschlussarbeit im Masterstudiengang Kern-, Teilchen und Astrophysik selbstständig und nur mit den angegebenen Hilfsmitteln angefertigt habe.

Christian Karl
Munich, 9th October 2018

Abstract

The neutrino is the second most abundant known particle in the universe, after the photon, and the knowledge of its absolute mass scale has a large impact on cosmological models as well as the nature of particle masses in general. While neutrino oscillation experiments have proven that neutrinos are not massless, they are only sensitive to the relative differences of individual mass eigenstates. A possibility to measure the absolute neutrino mass scale independently of the neutrino mass model is by studying the shape of the β -decay spectrum close to its endpoint. The **K**Arlsruhe **T**RITium Neutrino (KATRIN) experiment is designed to determine the effective electron neutrino mass using this method with a sensitivity of 200 meV (90 % CL).

First KATRIN tritium β -decay data was taken in May and June 2018. The goal of these measurements was to test analysis tools and probe the β -spectrum for systematic effects. In this thesis the first tritium data of KATRIN is analysed and various strategies for data and systematics handling are compared. For this purpose a new analysis tool *Fitritium* (Fit Tritium) was developed and applied to the data. Its main feature is that it is optimized for high-performance and the utilization of the analysis strategies discussed in this thesis. The analysis of this first measurement campaign with *Fitritium* demonstrated a very good agreement of the model predictions and the experimental spectrum. Most importantly, it could be shown that the effective endpoint of the β -spectrum is stable over time and distributed homogeneously over the individual pixels.

The focus of this thesis was to perform a detailed comparison of different techniques to combine data sets of several runs and detector pixels and to test various strategies of how to include systematic uncertainties. To combine the 148 detector pixels, three different techniques, namely the *uniform*, the *single-pixel* and the *multi-pixel* fit, were applied and the fit results were compared. All three agree within uncertainty for the sensitivity of first tritium. Two different options, *run appending* and *run stacking*, were tested for treating the data of multiple runs. The advantage of run appending is that it makes no approximation while run stacking eases data handling. For the statistics available in first tritium, no major difference in the fit results was found. In order to take systematic effects into account, the *nuisance parameter* and the *Monte Carlo propagation*, as well as the *covariance matrix method* was investigated. A combination of these techniques was successfully applied to a set of 27 runs corresponding to about three days of tritium data giving a comprehensive overview of the analysis results of this first measurement phase. The analysis code and strategies developed in this thesis will be of key importance for the forthcoming neutrino mass measurement starting in March 2019.

Contents

| | | |
|----------|---|-----------|
| 1 | Brief History of the Neutrino | 1 |
| 2 | The KATRIN Experiment | 3 |
| 2.1 | Neutrino Mass Determination from β -Decay | 3 |
| 2.2 | Molecular Tritium as β -Decay Source | 5 |
| 2.3 | Measuring Principle: MAC-E Filter Electron Spectroscopy | 5 |
| 2.4 | Experimental Setup | 6 |
| 2.4.1 | Rear Section | 7 |
| 2.4.2 | Windowless Gaseous Tritium Source | 7 |
| 2.4.3 | Pumping Sections | 8 |
| 2.4.4 | Pre- and Main-Spectrometer | 8 |
| 2.4.5 | Focal Plane Detector | 9 |
| 2.5 | Modelling of the Integrated β -Decay Spectrum | 10 |
| 2.5.1 | Final State Distribution | 10 |
| 2.5.2 | Doppler Effect | 11 |
| 2.5.3 | Response Function | 12 |
| 2.5.4 | Model of the Rate Expectation | 15 |
| 3 | Analysis Strategies | 16 |
| 3.1 | Maximum Likelihood Analysis | 16 |
| 3.2 | Pixel Combination | 18 |
| 3.2.1 | Uniform Fit | 18 |
| 3.2.2 | Single-Pixel Fit | 19 |
| 3.2.3 | Multi-Pixel Fit | 19 |
| 3.3 | Run Combination | 20 |
| 3.3.1 | Run Stacking | 20 |
| 3.3.2 | Run Appending | 21 |
| 3.3.3 | Multi-Run Analysis | 22 |
| 3.4 | Treatment of Systematic Effects | 23 |
| 3.4.1 | Nuisance Parameter Method | 23 |
| 3.4.2 | Monte Carlo Propagation of Uncertainty | 25 |
| 3.4.3 | Covariance Matrix Approach | 26 |

| | | |
|----------|---|-----------|
| 4 | New Analysis Tool: Fitrium | 28 |
| 4.1 | Physics Components | 28 |
| 4.2 | Code Structure | 29 |
| 4.3 | User Interface | 31 |
| 4.4 | Numerical Methods | 35 |
| 4.5 | Validation | 39 |
| 5 | Analysis of First Tritium Data | 40 |
| 5.1 | Initial Comparison of Model and Data | 41 |
| 5.2 | Parameter Stability over Time | 42 |
| 5.3 | Parameter Distribution over the Focal Plane Detector | 44 |
| 5.4 | Comparison of Analysis Strategies | 46 |
| 5.4.1 | Pixel Combination | 46 |
| 5.4.2 | Run Combination | 48 |
| 5.4.3 | Treatment of Systematic Effects | 50 |
| 5.5 | Analysis with Major Systematic Effects | 51 |
| 5.6 | Summary of Fit Results | 54 |
| 6 | Conclusion and Outlook | 56 |
| A | Slow Control Parameter Values for First Tritium Measurements | 62 |
| B | Derivation of Relative Number of Counts in Endpoint Region | 63 |
| C | In-Depth Code Explanation of Fitrium | 64 |
| D | Monte Carlo Generator for KATRIN | 69 |
| E | Additional Figures | 71 |

Chapter 1

Brief History of the Neutrino

The neutrino was postulated in 1930 by Wolfgang Pauli to describe the continuous electron energy spectrum observed in β -decay experiments. Over 20 years later, in 1956, it was experimentally confirmed by the Cowan-Reines neutrino experiment [1].

Since its discovery the understanding of the neutrino has increased tremendously and it is now well embedded in the Standard Model of particle physics. Neutrinos participate in the weak interaction, one of the three fundamental forces described by the Standard Model and the one responsible for β -decay. In correspondence with the charged leptons, the electron, the muon and tau, neutrinos come in three different flavours.

Various experiments have proven that it is possible for neutrinos to change their flavour by neutrino oscillations [2–4]. Neutrino oscillations arise from the fact that neutrino mass eigenstates are not equal to neutrino flavour eigenstates. Each flavour is composed of the three different mass states with a unique mixing described by the Pontecorvo-Maki-Nakagawa-Sakata (PMNS) matrix (1.1) [5, 6]. Differences in mass lead to a different propagation of the mass state components through space.

$$\begin{pmatrix} \nu_e \\ \nu_\mu \\ \nu_\tau \end{pmatrix} = \begin{pmatrix} U_{e1} & U_{e2} & U_{e3} \\ U_{\mu1} & U_{\mu2} & U_{\mu3} \\ U_{\tau1} & U_{\tau2} & U_{\tau3} \end{pmatrix} \begin{pmatrix} \nu_1 \\ \nu_2 \\ \nu_3 \end{pmatrix} \quad (1.1)$$

The probability to oscillate from one state i into another state j

$$P_{i \rightarrow j} \propto \sin^2 \left(\frac{\Delta m_{ij}^2 L}{4E} \right) \quad (1.2)$$

shows that neutrino oscillation experiments are only sensitive to the difference of the squared masses of two different mass states $\Delta m_{ij}^2 = m_i^2 - m_j^2$. The existence of neutrino oscillations

hence proves that neutrinos have mass, however the absolute mass scale of the neutrinos cannot be deduced from oscillation experiments.

Three methods to determine the absolute neutrino mass scale are currently being explored: cosmological investigation of large scale structure (LSS) formation and evolution [7], the search for neutrinoless double β -decay ($0\nu\beta\beta$) [8] and the analysis of the shape of the energy spectrum of electrons emitted by β -decay near the endpoint.

While the LSS analysis depends heavily on the cosmological model being used and $0\nu\beta\beta$ requires the neutrino to be a Majorana particle, the kinematics of β -decay do not depend on the neutrino mass model and are based on well-known physics. The **K**Arlsruhe **T**RITium Neutrino (KATRIN) experiment is designed to explore the absolute neutrino mass scale using this method with unprecedented sensitivity.

The high precision needed to reach KATRIN's design goals poses various challenges for the analysis of the data. This thesis studies strategies for the high-level analysis of the KATRIN experiment and presents results of the analysis of first KATRIN tritium data.

Chapter 2

The KATRIN Experiment

The Karlsruhe TRITium Neutrino (KATRIN) experiment is a next generation tritium β -decay experiment following the measurement principle of its predecessors in Mainz [9] and Troitsk [10]. It is designed to measure the effective electron anti-neutrino mass

$$m_\nu = \left(\sum_{i=1}^3 |U_{ei}|^2 \cdot m_i^2 \right)^{\frac{1}{2}} \quad (2.1)$$

with a sensitivity of 200 meV¹ at 90 % confidence level (C.L.).

This chapter gives an overview of the measurement principle of the KATRIN experiment with a focus on deriving a model used for analysis. Much more details on the experimental setup can be found in the KATRIN design report [11], the model builds upon [12].

2.1 Neutrino Mass Determination from β -Decay

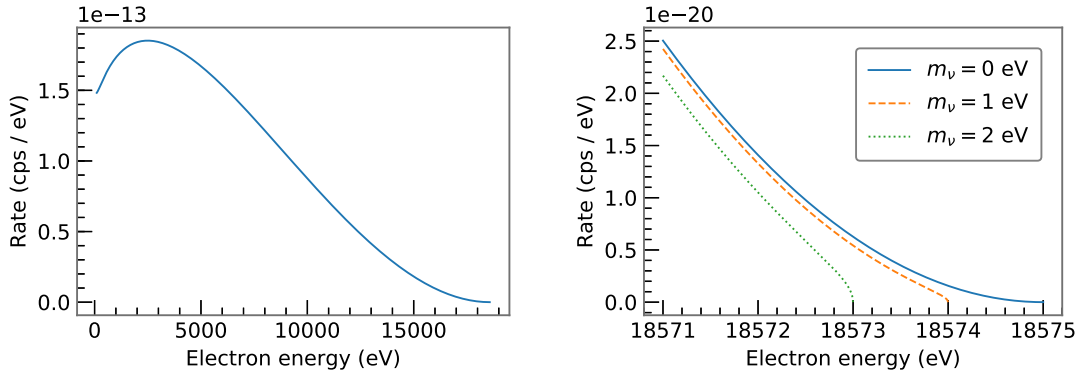
In a β^- -decay process a neutron in a nucleus X is transformed into a proton leaving over the daughter nucleus Y and emitting an electron e^- , an electron anti-neutrino $\bar{\nu}_e$ and the surplus energy Q :

$$X \rightarrow Y + e^- + \bar{\nu}_e + Q. \quad (2.2)$$

The released energy Q is shared between the decay products. The daughter nucleus Y is left with the recoil energy E_{rec} while the remaining energy, called the endpoint E_0 , is split between the electron and the anti-neutrino with corresponding energies E and E_ν respectively:

$$E_0 = Q - E_{\text{rec}} = E + E_\nu \quad (2.3)$$

¹This thesis uses natural units ($\hbar = c = 1$) for better readability



(a) Shape of spectrum in full range.

 (b) Impact of non-zero neutrino masses in E_0 region.

Figure 2.1: Differential tritium β -spectrum in dependence of electron energy.

As the energy of the neutrino E_ν is given by

$$E_\nu = \sqrt{m_\nu^2 + p_\nu^2}, \quad (2.4)$$

a neutrino with non-zero rest mass always takes some of the released energy and hereby reduces the maximal energy E the electron can receive. Equation (2.5) gives the differential rate for an allowed β -decay in dependence of the electron energy E [13]:

$$\frac{d\Gamma}{dE} = C \cdot F(Z', E) \cdot p \cdot (E + m_e) \cdot (E_0 - E) \cdot \sqrt{(E_0 - E)^2 - m_\nu^2} \cdot \Theta(E_0 - E - m_\nu). \quad (2.5)$$

Here the constant

$$C = \frac{G_F^2 \cos^2 \theta_C}{2\pi^3} \cdot |M_{\text{nuc}}|^2 \quad (2.6)$$

incorporates the Fermi constant G_F , the Cabbibo angle θ_C and the nuclear matrix element M_{nuc} , $F(Z', E)$ is the Fermi function that accounts for electromagnetic interaction of the outgoing electron with the daughter nucleus and the Heaviside function Θ assures energy conservation. This dependence is shown in figure 2.1a while the impact of non-zero neutrino masses on the β -spectrum shape in the endpoint region is displayed in figure 2.1b.

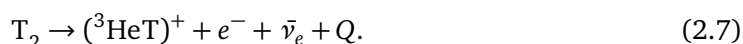
As one can deduce from figure 2.1b, measuring the differential spectrum in the endpoint region with sub-eV precision is an option to determine the absolute neutrino mass scale. From the magnitude of the impact it is clear that one requires an experiment with excellent energy resolution in the eV range and the very low rates in the endpoint region show that a highly luminous source is needed. Both needs are fulfilled in the KATRIN experiment and are explained in section 2.3.

2.2 Molecular Tritium as β -Decay Source

Tritium as a β -emitter has various advantageous properties for a β -decay experiment [14]:

- Its endpoint value of $E_0 \approx 18.6$ keV [13] is the second lowest of all isotopes undergoing β -decay. A low endpoint value is advantageous as it leads to relatively more counts in the endpoint region in which the neutrino mass manifests itself² and for technical reasons as it requires lower voltages in operation of the MAC-E filter described in section 2.3.
- The tritium decay is a super-allowed transition which leads to a rather short half-life of $T_{1/2} = 12.3$ years with correspondingly high rates at low source densities. Additionally the nuclear matrix element is energy independent and easy to calculate.
- In its molecular form T_2 , tritium can be used in gaseous state at low temperatures. This state is preferred as systematic uncertainties are decreased and higher rates are achievable.

Since KATRIN uses tritium in its molecular form, tritium β -decay is described by



2.3 Measuring Principle: MAC-E Filter Electron Spectroscopy

The operation principle of KATRIN is an integral measurement of the tritium β -spectrum using magnetic adiabatic collimation (MAC) and an electrostatic (E) high-pass filter. It is depicted in figure 2.2.

Electrons emitted in the source with magnetic field B_S are guided along the magnetic field lines towards the center of the spectrometer and perform a cyclotron motion superimposed to their movement along the magnetic field. The magnetic field in the spectrometer B_{\min} is several orders of magnitude smaller which creates a magnetic field gradient. As the magnetic flux $\Phi = B \cdot A$ is constant, the spectrometer must be much larger than the source. Electron momentum perpendicular to the field line p_{\perp} is transformed into momentum parallel to the field line p_{\parallel} adiabatically, meaning electron orbital momentum is conserved, along this gradient (shown in orange).

A large voltage U in the order of 18 kV is applied at the minimum magnetic field which creates an electrostatic barrier with energy qU (shown in green). Only electrons with transver-

²See appendix B for a quick derivation.

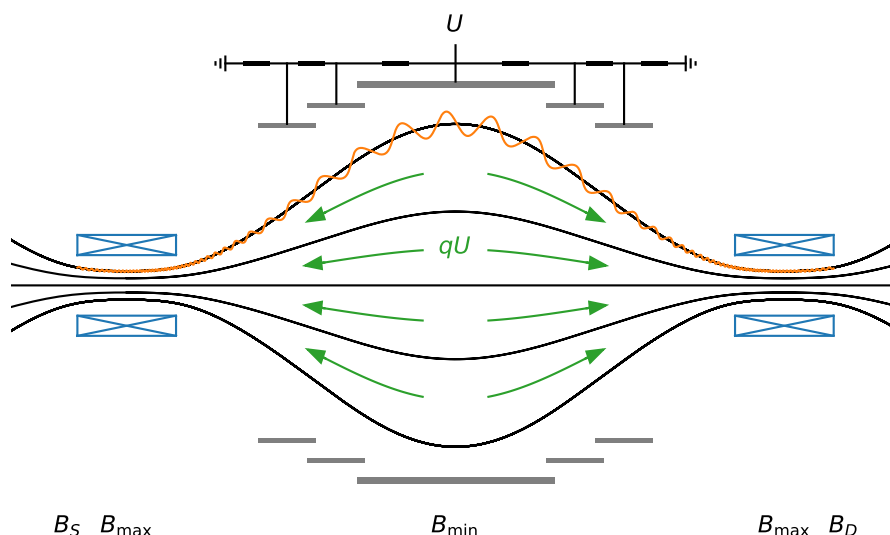


Figure 2.2: Principle of the MAC-E filter, figure adapted from [15].

sal energy $E_{\parallel} \geq qU$ pass this barrier and are re-accelerated towards the detector leading to the integral measurement of the decay spectrum.

If the source was positioned at maximum magnetic field, all electrons emitted in direction of the spectrometer would be accepted or in other words the accepted solid angle $\frac{\Omega}{4\pi} = \frac{1}{2}$. In practice this is unfavourable as electrons with large starting angles travel long distances in the source which increases their probability to scatter. Therefore the source is placed at a lower magnetic field $B_S < B_{\max}$ leading to a reduced maximum acceptance angle by the magnetic mirror effect of

$$\theta_{\max} = \arcsin \sqrt{\frac{B_S}{B_{\max}}} \quad (2.8)$$

and a correspondingly decreased solid angle of

$$\frac{\Omega}{4\pi} = \frac{1 - \cos \theta_{\max}}{2}. \quad (2.9)$$

2.4 Experimental Setup

An overview of the experimental setup is given in figure 2.3. Each element is briefly described in the following paragraphs.

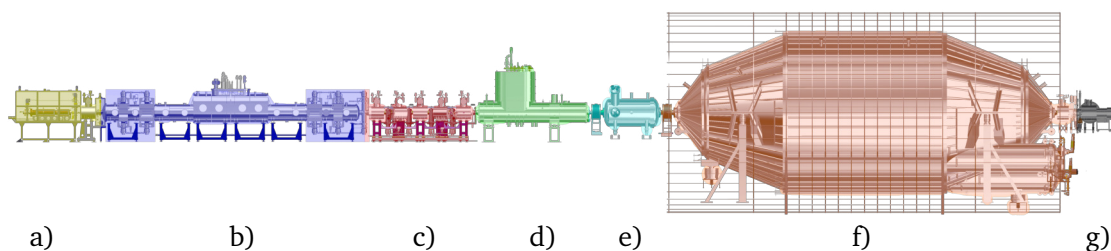


Figure 2.3: Overview of the KATRIN experiment with the main components:

- a) Rear section
- b) Windowless gaseous tritium source (WGTS)
- c) Differential pumping section (DPS)
- d) Cryogenic pumping section (CPS)
- e) Pre-spectrometer (PS)
- f) Main-spectrometer (MS)
- g) Focal plane detector (FPD)

2.4.1 Rear Section

Main purpose of the rear section is to supply a defined electric potential of the tritium gas in the source by providing a conducting surface, the rear wall. In addition it houses monitoring and calibration tools. [16]

2.4.2 Windowless Gaseous Tritium Source

The windowless gaseous tritium source (WGTS) [17] is an ultra stable and highly luminous gaseous tritium source consisting of a stainless steel tube of $l_S = 10$ m length and $d_S = 90$ mm diameter. Tritium gas of high purity $\epsilon_T \geq 95\%$ is continuously injected into the source through more than 250 holes at its centre. The gas then freely streams to both ends and is pumped away by multiple turbo-molecular pumps and then fed into a sophisticated loop system which reprocesses and re-injects the tritium.

To obtain a high tritium density at reasonable pressure and flow rate and to reduce the effects of Doppler broadening, the source is operated at a low temperature of about 30 K.

The number of molecules in the source is described by the column density ρd which is the gas density integrated over the source length. It is related to the total number of tritium atoms in the source by

$$N_{\text{tot}} = 2 \cdot A_S \cdot \rho d \quad (2.10)$$

where the factor two accounts for the number of atoms in a T_2 molecule and A_S is the source

area given by

$$A_S = \pi \cdot \left(\frac{d_S}{2}\right)^2. \quad (2.11)$$

In operation only part of the source area is mapped to the detector to avoid electrons which scattered on the source tube. The effective source area can be retrieved via the magnetic flux and the magnetic field in the source:

$$A_{\text{eff}} = \frac{\Phi}{B_S}. \quad (2.12)$$

This reduces the effective number of atoms seen to:

$$N_{\text{eff}} = 2 \cdot A_{\text{eff}} \cdot \rho d. \quad (2.13)$$

During the recent KATRIN tritium campaign the magnetic field of the source was $B_S = 2.52$ T and the column density was $\rho d \approx 4.5 \times 10^{21} \text{ m}^{-2}$. The maximum magnetic field setting $B_{\text{max}} = 4.2$ T leads to the maximum acceptance angle $\theta_{\text{max}} \approx 50.77^\circ$ using (2.8).

2.4.3 Pumping Sections

Tritium from the source may not reach the spectrometers as decay processes in the spectrometers would be a major source of background. The task of the pumping sections is to reduce the tritium flow rate by 14 orders of magnitude in combination with the source which already achieves a reduction by a factor of 100.

A reduction by more than a factor of 10^5 is achieved by the differential pumping section (DPS) [18] which uses turbo-molecular pumps (TMPs). The remaining reduction is achieved by passive adsorption of tritium molecules onto the tube surfaces in the cryogenic pumping section (CPS) [19] operated at a temperature of 4.5 K. These cold surfaces are covered by a thin argon frost layer to enhance the trapping probability of tritium molecules.

Both pumping sections are built in a chicane shape. Electrons are guided adiabatically by magnetic fields through the turns while uncharged molecules hit the wall and are pumped away or adsorbed.

2.4.4 Pre- and Main-Spectrometer

Both the pre- and the main-spectrometer are built following the MAC-E filter principle described in 2.3.

The smaller pre-spectrometer is operated at a retarding energy of around 300 eV less in absolute value than the main spectrometer. It thus acts as a pre-filter rejecting the majority of uninteresting electrons that would not make it past the main spectrometer for background reduction.

Core of the KATRIN experiment is the large main spectrometer with a diameter of 10 m. Its energy resolution is determined by the magnetic field settings:

$$\frac{\Delta E}{E} = \frac{B_{\min}}{B_{\max}}. \quad (2.14)$$

For the recent KATRIN tritium campaign the minimum magnetic field in the analysing plane of the main spectrometer was $B_{\min} = 6 \times 10^{-4}$ T leading to an energy resolution of $\Delta E \approx 2.7$ eV using (2.14) and assuming an electron energy of 18.6 keV.

2.4.5 Focal Plane Detector

The electrons that pass the main spectrometer are re-accelerated due to the MAC-E filter and further post-acceleration, as high energy electrons are easier to detect and to shift the spectrum above detector-related background, and guided to the focal plane detector (FPD) [20]. The detector is a multi-pixel silicon semiconductor detector with an energy resolution of around 1.4 keV (FWHM) per pixel. The 148 pixels of equal area are arranged in a dart-board shape as shown in figure 2.4. Each pixel counts the number of electrons detected. The radial and azimuthal segmentation allows to correct for inhomogeneities in source, magnetic and electric fields. The efficiency of the detector $\epsilon_{\text{detector}}$ is determined by the region of interest (ROI) cut and physical effects such as back-scattering. Typical values are within 0.9 to 0.95.

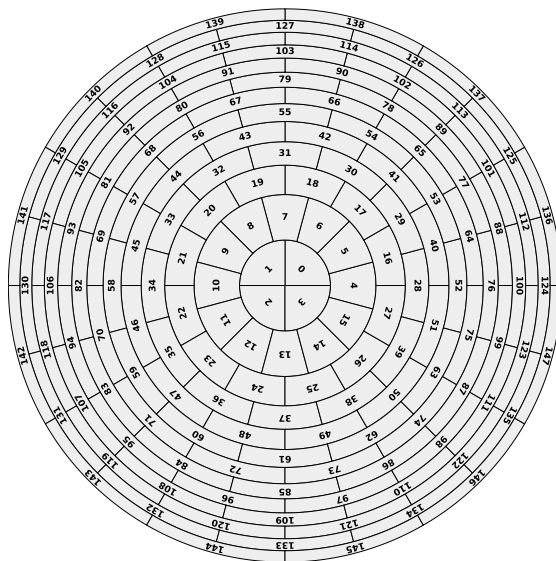


Figure 2.4: Pixel segmentation of the focal plane detector.

2.5 Modelling of the Integrated β -Decay Spectrum

This section focusses on deriving a model of the integrated β -decay spectrum describing the expected rate of the KATRIN experiment. First, two effects modifying the differential rate $\frac{d\Gamma}{dE}$ are explained. Afterwards the response of the KATRIN setup is discussed and finally these components are combined to a complete model of the rate expectation.

2.5.1 Final State Distribution

As described in section 2.2, KATRIN uses tritium in its molecular form as β -decay source. Therefore the daughter molecule can be in a rotational-vibrational or electronic excited state with energy V_f and corresponding probability P_f . This modifies equation (2.5) as the effective maximum energy available for electron and neutrino shifts away from the endpoint: $E_0 \rightarrow E_0 - V_f$. Introducing $\epsilon_f = E - E_0 - V_f$ the decay rate now reads as

$$\frac{d\Gamma}{dE} = C \cdot F(Z', E) \cdot p \cdot (E + m_e) \cdot \sum_f P_f \cdot \epsilon_f \cdot \sqrt{\epsilon_f^2 - m_\nu^2} \cdot \Theta(\epsilon_f - m_\nu). \quad (2.15)$$

Precise knowledge of the distribution of these final states is of high importance for neutrino mass measurements as inaccuracies can lead to a biased neutrino mass result. The final state distribution (FSD) can be calculated from theory as done for example by Saenz et al. [21]. An excerpt of the FSD of $({}^3\text{HeT})^+$ is shown in figure 2.5.

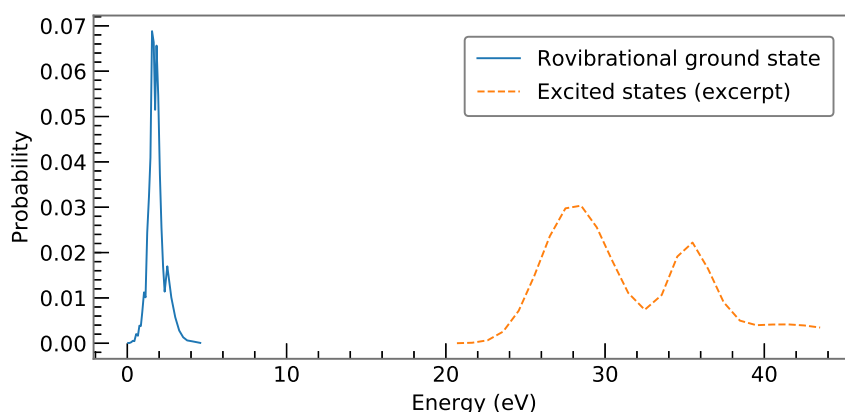


Figure 2.5: Final state distribution of $({}^3\text{HeT})^+$ according to A. Saenz et al. [21]. The distribution is split into two parts: the rovibrational ground state (blue) and the excited states (orange).

It is clearly split into two parts:

- the rovibrational ground state centred at 1.7 eV with a Gaussian width of about 0.36 eV
- and a set of electronic excited states with energies > 20 eV.

2.5.2 Doppler Effect

Additionally, since the tritium molecules in the source are in thermal motion, the differential spectrum is broadened by the Doppler effect. This can be described by convolving the differential spectrum (2.15) with a Maxwellian distribution g :

$$\frac{d\Gamma}{dE}(E) \rightarrow \int_{-\infty}^{\infty} g(E - \epsilon) \frac{d\Gamma}{dE}(\epsilon) d\epsilon. \quad (2.16)$$

In its non-relativistic approximation g is described by a normal distribution

$$g(E - \epsilon) = g(\Delta E) = \frac{1}{\sqrt{2\pi}\sigma_E} \cdot \exp\left(-\frac{\Delta E^2}{2\sigma_E^2}\right) \quad (2.17)$$

with the broadening width

$$\sigma_E = \sqrt{2Ek_B T \frac{m_e}{m_{T_2}}} \quad (2.18)$$

depending on the energy of the emitted electron E , the Boltzmann constant k_B , the source temperature T and the mass ratio of the electron and T_2 . Inserting values typical for the KATRIN experiment, $E = E_0 \approx 18.6 \text{ keV}$, $T = 30 \text{ K}$, leads to a broadening of $\sigma_E = 93.5 \text{ meV}$.

At the sensitivity of first tritium measurements, the effect of Doppler broadening on the model of the rate expectation is negligible.

2.5.3 Response Function

The response function $R(qU, E)$ describes the probability of an electron with energy E to pass the MAC-E filter at a given retarding energy qU . In an ideal apparatus without energy loss it would consist of a simple step function:

$$R(qU, E) = \begin{cases} 0 & E < qU \\ 1 & E \geq qU. \end{cases} \quad (2.19)$$

In the KATRIN experiment two effects dominate the response function: the transmission function of the MAC-E filter and energy loss due to scattering effects in the source.

Not all the perpendicular momentum of an electron is converted to momentum parallel to the electric field in the spectrometer. Therefore also electrons with $E \geq qU$ may not pass the electrostatic barrier. The transmission probability can be described by

$$T(qU, E) = \begin{cases} 0 & E < qU \\ \frac{1 - \sqrt{1 - f \cdot \frac{B_S}{B_{\min}} \cdot \frac{E - qU}{E}}}{1 - \sqrt{1 - \frac{B_S}{B_{\max}}}} & qU \leq E \leq qU \frac{f \cdot B_{\max}}{f \cdot B_{\max} - B_{\min}} \\ 1 & E > qU \frac{f \cdot B_{\max}}{f \cdot B_{\max} - B_{\min}} \end{cases} \quad (2.20)$$

with the relativistic factor

$$f = \frac{\frac{E - qU}{m_e} + 2}{\frac{E}{m_e} + 2}. \quad (2.21)$$

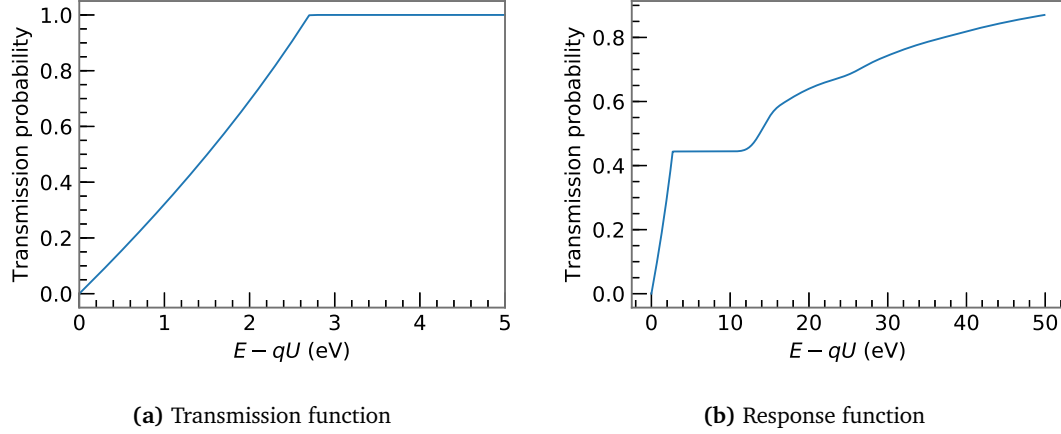
The shape of the transmission function is shown in figure 2.6a for the parameter values during first tritium measurements (see table A.1 in the appendix).

The major energy loss component is inelastic scattering of electrons with tritium molecules in the source. The probability of an electron to scatter i -times is described by

$$P_i = \frac{1}{1 - \cos \theta_{\max}} \int_0^{\theta_{\max}} \sin(\theta) \int_0^1 P_{\text{inel},i}(z, \theta) dz d\theta. \quad (2.22)$$

Table 2.1: Scattering probabilities in percent

| P_0 | P_1 | P_2 | P_3 | P_4 | P_5 | P_6 | P_7 | P_8 | P_9 | P_{10} |
|-------|-------|-------|-------|-------|-------|-------|-------|-------|-------|----------|
| 44.42 | 29.58 | 15.65 | 6.785 | 2.487 | 0.790 | 0.221 | 0.056 | 0.012 | 0.003 | 0.001 |


Figure 2.6: Shape of transmission and response function for first tritium measurements.

with the inelastic scattering probability

$$P_{\text{inel},i}(z, \theta) = \frac{(\lambda(z, \theta) \cdot \sigma_{\text{inel}})^i}{i!} \cdot e^{-\lambda(z, \theta) \cdot \sigma_{\text{inel}}}, \quad \lambda(z, \theta) = \frac{z \cdot \rho d}{\cos \theta} \quad (2.23)$$

assuming no angular change after scattering. The energy-dependent inelastic scattering cross section [22] is given by

$$\sigma_{\text{inel}}(E) = \frac{4\pi a_0^2}{E/R} \left[1.5487 \ln \left(\frac{\beta^2}{1 - \beta^2} \right) + 17.4615 \right] \quad (2.24)$$

with the Bohr radius a_0 and the rydberg energy R . The scattering probabilities zero to ten are listed in table 2.1 assuming a column density value of $\rho d = 4.5 \times 10^{21} \text{ m}^{-2}$ and an energy $E = 18575 \text{ eV}$.

The energy ϵ lost by i -fold scattering can be described by the energy loss function $f_i(\epsilon)$. An electron that does not scatter, loses no energy. Its energy loss function is therefore simply a Dirac δ -function:

$$f_0(\epsilon) = \delta(\epsilon). \quad (2.25)$$

Electrons that scatter once lose energy according to

$$f_1(\epsilon) = \begin{cases} A_1 \cdot \exp\left(-2\left(\frac{\epsilon - \epsilon_1}{\omega_1}\right)^2\right) & \epsilon < \epsilon_C \\ A_2 \cdot \frac{\omega_2^2}{\omega_2^2 + 4(\epsilon - \epsilon_2)^2} & \epsilon \geq \epsilon_C \end{cases} \quad (2.26)$$

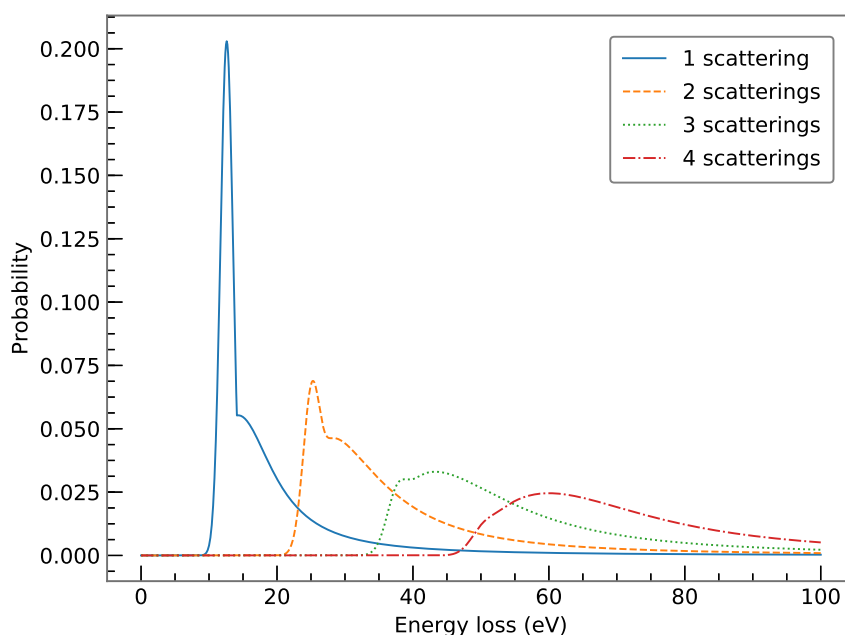


Figure 2.7: Energy loss function according to [23, 24]. The function for 1 scattering (blue) is the representation of (2.26). Higher order functions are retrieved by convolving this function with itself (orange, green, red).

where the Gaussian part comes from excitation processes and the Lorentzian part from ionization of tritium molecules [23, 24]. Energy loss functions for $i \geq 2$ scatterings can be obtained by convolving (2.26) $(i - 1)$ -times with itself. The energy loss functions for one to four scatterings are displayed in 2.7. This simple analytical energy loss function is not precise enough for KATRIN's design sensitivity. Therefore there will be dedicated electron gun measurements to determine the energy loss function using a deconvolution approach [25].

The total response function is then composed as a convolution of the transmission function with the energy loss function.

$$R(qU, E) = \int_0^{E-qU} T(qU, E - \epsilon) \sum_{i=0}^{\infty} P_i \cdot f_i(\epsilon) d\epsilon \quad (2.27)$$

In practice 5 to 10 scatterings are considered depending on the size of the analysis window. Scattering more often is highly unlikely as can be seen in table 2.1. An example of the response function is shown in figure 2.6b.

2.5.4 Model of the Rate Expectation

As mentioned at the beginning of this chapter, KATRIN measures an integrated tritium β -spectrum. The shape is composed of the differential spectrum $\frac{d\Gamma}{dE}(E)$ described in (2.15) and the response function $R(qU, E)$ derived in (2.27):

$$I(qU) = C \cdot \int_{qU}^{E_0} \frac{d\Gamma}{dE}(E) \cdot R(qU, E) dE \quad (2.28)$$

with the constant prefactor C

$$C = N_{\text{eff}} \cdot \frac{1 - \cos \theta_{\text{max}}}{2} \cdot \epsilon_{\text{detector}} \quad (2.29)$$

consisting of the effective number of tritium atoms in the source N_{eff} (2.13), the solid angle (2.9) and the detector efficiency $\epsilon_{\text{detector}}$.

In addition to the signal, a constant background rate B is expected. The total rate is then

$$\Gamma(qU) = I(qU) + B = C \cdot \int_{qU}^{E_0} \frac{d\Gamma}{dE}(E) \cdot R(qU, E) dE + B \quad (2.30)$$

Chapter 3

Analysis Strategies

The goal of the KATRIN experiment is to infer a value or upper limit for the effective electron anti-neutrino neutrino mass. To this end methods of statistical parameter inference, data combination and treatment of systematic uncertainties are required. In this chapter an overview of all the techniques considered for neutrino mass analysis is given.

3.1 Maximum Likelihood Analysis

The likelihood function \mathcal{L} is used in statistical methods of parameter inference. It describes how probable a specific outcome of an experiment x is given a model μ . The model itself can depend on a set of parameters $\vec{\theta}$. The likelihood function then reads as

$$\mathcal{L} = \mathcal{L}(\mu(\vec{\theta}); x) = \mathcal{L}(\vec{\theta}; x). \quad (3.1)$$

To retrieve the model that best describes the data, a set of parameters $\vec{\theta}$ is found such that it maximizes the likelihood function.

We now infer the basic likelihood function describing KATRIN data. In KATRIN an integrated tritium β -decay spectrum is measured. As the decay process itself is stochastic, the number of expected decays and hence the number of expected electron counts is described by a probability distribution function (PDF). Assuming the decay rate in the source is constant and the individual decays are independent of one another, the underlying PDF of the number of decays is the Poisson distribution in equation (3.2). It describes the probability to observe N counts given an average model prediction $\mu(\vec{\theta})$:

$$P(N \text{ counts}; \mu(\vec{\theta})) = e^{-\mu(\vec{\theta})} \frac{\mu^N(\vec{\theta})}{N!}. \quad (3.2)$$

Thus $\mathcal{L}(\mu(\vec{\theta}); N) = P(N; \mu(\vec{\theta}))$ is the likelihood function of the parameters $\vec{\theta}$ for a single point of the tritium β -spectrum. The model prediction μ includes the differential tritium spectrum and modelling of the KATRIN apparatus as described in (2.30).

The entire spectrum consists of many counts N_i measured at given different retarding energies qU_i . The individual points are statistically independent and therefore the joint probability distribution P_{total} for the whole spectrum is the product of the individual PDFs

$$P_{\text{total}}(\vec{\mu}; \vec{N}) = \prod_i e^{-\mu_i} \frac{\mu_i^{N_i}}{N_i!}, \quad (3.3)$$

where i runs over all retarding energies and μ_i is defined as $\mu(qU_i; \vec{\theta})$.

In practice it is numerically favorable to minimize $-\ln \mathcal{L}$ instead of maximizing \mathcal{L} as the product of many small numbers quickly leads to numerical difficulties. In addition, taking derivatives of a sum is much easier than taking derivatives of a product.

For large model predictions μ the Poisson distribution asymptotically tends to the normal distribution with mean μ and standard deviation $\sqrt{\mu} \approx \sqrt{N}$:

$$P(N \text{ counts}, \mu) = \frac{1}{\sqrt{2\pi N}} e^{-\frac{(N-\mu)^2}{2N}}. \quad (3.4)$$

In this case minimizing $-\ln \mathcal{L}$ is equivalent to the well-known χ^2 -minimization:

$$\begin{aligned} -\ln \mathcal{L}(\vec{\mu}; \vec{N}) &= -\ln \left(\prod_i \frac{1}{\sqrt{2\pi N_i}} e^{-\frac{(N_i - \mu_i)^2}{2N_i}} \right) \\ &= -\sum_i \ln \left(\frac{1}{\sqrt{2\pi N_i}} e^{-\frac{(N_i - \mu_i)^2}{2N_i}} \right) \\ &\propto -\sum_i \ln \left(e^{-\frac{(N_i - \mu_i)^2}{2N_i}} \right) \\ &= \sum_i \frac{(N_i - \mu_i)^2}{2N_i} \\ &=: \frac{1}{2} \chi^2(\vec{\mu}; \vec{N}). \end{aligned}$$

In a basic model there are four free parameters in $\vec{\theta}$: the neutrino mass squared m_ν^2 , the endpoint value E_0 , the normalization of the spectrum A_S and the constant background rate B . An additional parameter ΔqU can be introduced to describe the difference of the WGTS and main spectrometer work function arising from plasma effects in the source and inhomogeneities in the spectrometer. The model prediction at given retarding energy qU and measuring time t then is described by

$$\mu(qU, t; m_\nu^2, E_0, A_S, B, \Delta qU) = A_S \cdot t \cdot \int_{qU + \Delta qU}^{E_0} \frac{d\Gamma(E; m_\nu^2, E_0)}{dE} \cdot R(qU + \Delta qU, E) dE + B \cdot t. \quad (3.5)$$

3.2 Pixel Combination

The KATRIN focal plane detector is segmented into 148 pixels as described in 2.4.5. Each pixel measures a statistically independent β -spectrum. In addition to their statistical independence, the spectra of each pixel differ due to inhomogeneities in source and fields in the analyzing plane.

To retrieve one final value for the physical parameters like the neutrino mass squared the spectra from all pixels must be combined. In the following three different methods for pixel combination are described and their advantages and disadvantages discussed.

3.2.1 Uniform Fit

The simplest way to combine the spectra of multiple pixels is to add the counts in each pixel and fit with a single averaged model. Apart from that, this requires:

- averaging the retarding energies seen by the different pixels,
- averaging any slow control parameters differing between the pixels, for example the magnetic field in the analyzing plane
- and averaging the live time of each pixel.

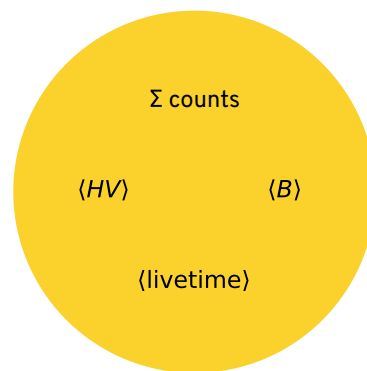


Figure 3.1: Scheme of uniform fit.

Averaging slow control parameters is an approximation which is too simplified for final neutrino mass analysis as it leads to a large shift of the neutrino mass squared. This is shown in table 1 of [12, p. 17], especially by the radial dependence of the retarding energy. Nevertheless the uniform fit approach is usable in case the statistical uncertainty dominates over the systematic shift of m_ν^2 .

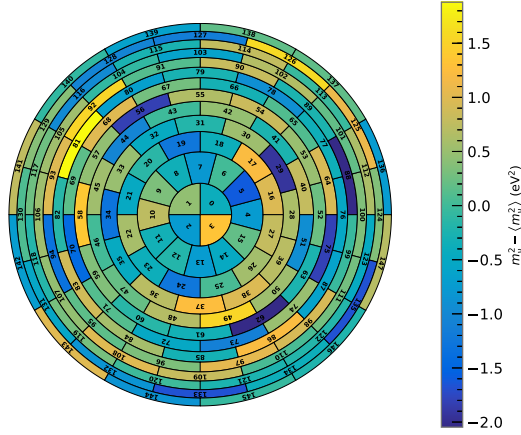


Figure 3.2: Distribution of m_ν^2 over the KATRIN detector for arbitrary Monte Carlo data. The result $m_\nu^2 = 122 \pm 66 \text{ meV}^2$ is retrieved using sample mean and error on the mean.

3.2.2 Single-Pixel Fit

Another intuitive way to treat the spectra of multiple pixels is to fit each of them individually. Therefore:

- each pixel is assigned its own model
- and the likelihoods of the individual pixels are treated independently.

A single value per pixel is retrieved for the fit parameters. In this case one is left with 148 values for the neutrino mass squared m_ν^2 and the endpoint E_0 , although there is only one value for each in nature (see figure 3.2). The most straightforward way to retrieve a single value with an uncertainty is to use the sample mean and sample variance assuming that the distribution is Gaussian. This assumption may not be valid, especially if there are underlying systematic effects.

3.2.3 Multi-Pixel Fit

To handle the shortcoming of the single-pixel fit, namely the difficulty of combining the individual results, one can combine the likelihoods of the separate pixels in one large likelihood \mathcal{L}_{multi} with parameters shared between pixels:

$$\mathcal{L}_{multi} = \prod_{i=0}^{N_{pixels}-1} \mathcal{L}_i = \mathcal{L}_0(m_\nu^2, E_0, A_{S,0}, B_0) \cdot \mathcal{L}_1(m_\nu^2, E_0, A_{S,1}, B_1) \cdot \dots \quad (3.6)$$

Here the neutrino mass squared m_ν^2 and the endpoint E_0 are shared parameters, the signal amplitude A_S and the background rate B are pixel dependent. The total number of free parameters is then $2 + 2 \cdot 148 = 298$.

In this case:

- each pixel is assigned its own model,
- the combined likelihood for all pixels is maximized
- and we obtain a single fit result for shared parameters.

The multi-pixel fit therefore automatically provides a single fit result for the physical parameters of interest while still using a different model for each pixel to account for pixel-dependent effects. The downside of this approach is the large number of free parameters and thus the increased complexity of the fit.

3.3 Run Combination

The KATRIN experiment will measure the integrated tritium spectrum several thousands of times. We define each measurement of the spectrum as a “run” while the data taken at a set retarding energy within one run is called “subrun”. The data of all of the runs must be combined to retrieve a final neutrino mass result. This section discusses two simplified options for run combination that can be applied when the slow control parameters were stable in all runs combined. The more complicated case of varying slow control parameters is briefly mentioned at the end of the section for completeness.

3.3.1 Run Stacking

In each run the same retarding energies are applied. The data points at same retarding energies can be “stacked”, meaning the counts and measuring time of the data points are added to create a single data point from them.

However, due to the finite precision of the KATRIN high-voltage system, the set retarding energies may not coincide within the sub-ppm measurement accuracy over prolonged periods of time. This leads to different retarding energies in the spectra being combined which must then be averaged for the stacked data point.

The stacking process is displayed for one subrun in figure 3.3. One can see the lowering of

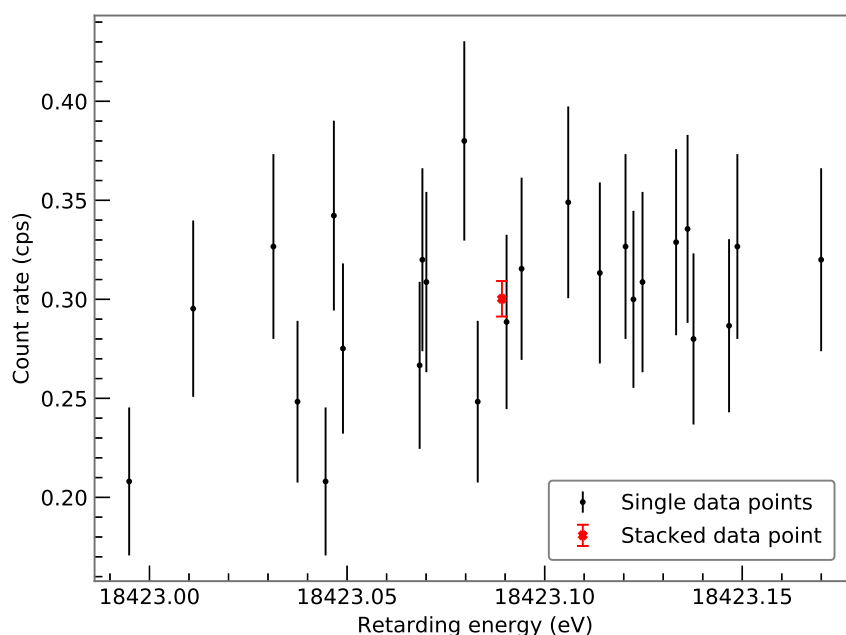


Figure 3.3: Stacking of data points within one subrun. The black points show the actual retarding energy reading at a given setting from multiple spectra. The red point is the result of the stacking process.

the statistical uncertainty due to the stacking of multiple data points and the necessity for averaging the retarding energy because of the spread between the single measurements.

The advantage of stacking is that it greatly reduces the number of points in the analysed spectrum, leading to a faster analysis process. The downside is the energy scale distortion induced by the averaging of retarding energies. As derived for example in [15], a distortion with variance σ^2 leads to a shift of the neutrino mass squared by $-2\sigma^2$. This is an additional systematic effect which adds to the total systematic budget of the experiment.

3.3.2 Run Appending

Another way to combine the data points of multiple spectra is to combine them as part of one large spectrum as visualized in figure 3.4. The complete spectrum can now be analysed in one likelihood including all the data points:

$$\mathcal{L}_{\text{appended}} = \prod_{i=1}^{N_{\text{runs}}} \mathcal{L}_i. \quad (3.7)$$

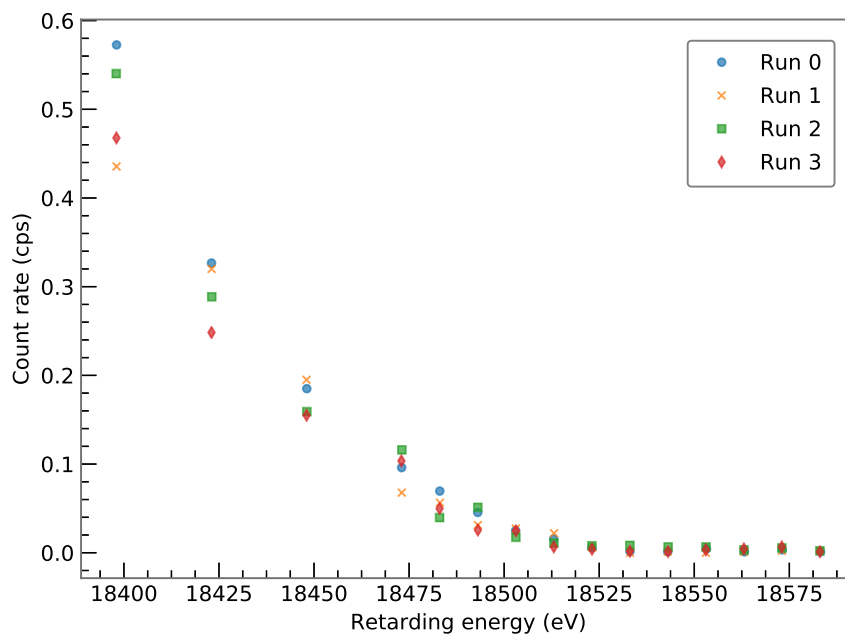


Figure 3.4: Appending of four runs to create one large spectrum. The different types of data points correspond to different runs.

This method does not lead to an energy scale distortion as the method described in 3.3.1 but it complicates data handling and fitting due to the large number of data points analysed at once.

3.3.3 Multi-Run Analysis

In case the slow control parameters of multiple runs vary, two options similar to the pixel combination are possible: fitting each run individually and combining the results or creating a combined likelihood with shared parameters between runs. In analogy to the pixel combination the first approach is called single-run fit where the second is a multi-run fit.

3.4 Treatment of Systematic Effects

Within the framework of maximum likelihood estimation, let us discuss three options that were considered for the KATRIN data analysis.

3.4.1 Nuisance Parameter Method

The first method discussed is the so called nuisance parameter or pull term method. The model is extended by including additional parameters $\vec{\theta}_{\text{systematic}}$, such as ρd or B -fields, that are free in the minimization. Furthermore, the additional nuisance parameters are constrained by so-called pull terms in the likelihood function.

Pull terms $f(\vec{\theta}_{\text{systematic}})$ are additional terms in the likelihood that only depend on the value of the systematic parameters $\vec{\theta}_{\text{systematic}}$ they constrain. Their function f is determined by the knowledge of the systematic parameters which can be obtained for instance by calibration measurements.

The general procedure for the pull term method is:

1. Start with initial likelihood without systematic uncertainties $\mathcal{L}_{\text{init}}(\vec{\theta}_{\text{init}})$.
2. Introduce additional free parameters for the systematic uncertainties

$$\mathcal{L}_{\text{init}}(\vec{\theta}_{\text{init}}) \rightarrow \mathcal{L}_{\text{init}}(\vec{\theta}_{\text{init}}, \vec{\theta}_{\text{systematic}}) = \mathcal{L}_{\text{init}}(\vec{\theta}).$$

3. Constrain systematic parameters with pull terms $f(\vec{\theta}_{\text{systematic}})$

$$\mathcal{L}_{\text{total}}(\vec{\theta}) = \mathcal{L}_{\text{init}}(\vec{\theta}) \cdot f(\vec{\theta}_{\text{systematic}}).$$

A typical pull term is the normal distribution for one parameter with Gaussian uncertainty σ and best value μ :

$$f(\theta) = \frac{1}{\sqrt{2\pi}\sigma} e^{-\frac{(\theta-\mu)^2}{2\sigma^2}}. \quad (3.8)$$

The introduced additional freedom of the fit increases the uncertainty on the fit parameters accordingly. This broadening is shown in figure 3.5.

The method itself is straightforward and easy to implement. A great advantage of this approach is that by including the systematic parameters in the fit, the data can be used to

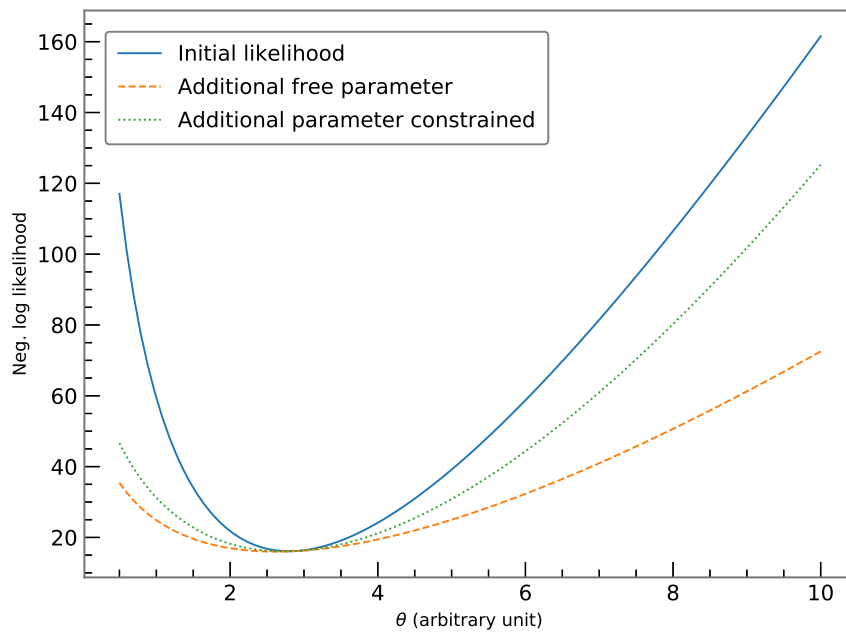


Figure 3.5: Change of likelihood shape by introducing a pull term using a toy model. By adding an additional free parameter the initial likelihood (blue) broadens significantly (orange). Constraining this additional free parameter with a pull term decreases the width of the likelihood again (green).

learn something about them. Main drawback of the pull term method is the increase of the number of fit parameters and with it the increased complexity of the fit.

3.4.2 Monte Carlo Propagation of Uncertainty

Another option for the propagation of systematic uncertainties into the fit result is to propagate the distribution of the systematic parameter into the distribution of the fit parameters using a Monte Carlo sampling method. This approach can be described by a three step process also shown in figure 3.6:

1. Draw value of the systematic parameter from a given distribution.
2. Fit with the chosen value of the systematic parameter fixed and retrieve the results.
3. Repeat the process often to retrieve the distribution of the fit parameters.

The width of the retrieved distribution of the fit parameters reflects their systematic uncertainty σ_{sys} . This can then be added to the statistical uncertainty σ_{stat} of the initial fit to retrieve the total uncertainty $\sigma_{\text{tot}} = \sqrt{\sigma_{\text{stat}}^2 + \sigma_{\text{sys}}^2}$.

To propagate multiple uncertainties and keep track of correlations, multiple parameters are varied at once in the first step. The complexity of the Monte Carlo propagation hence does not depend on the number of systematic parameters and can be extended easily. In addition, as all N fits are independent, they can be parallelized to speed up the process.

The main downside of the Monte Carlo propagation is that it does not allow learning about the systematic parameters themselves from the data. They are plugged in with a given distribution and the final results do not include any additional information on the systematics. This drawback is especially obvious if the true value of the systematic parameter is shifted compared to the expectation. In the MC approach the expectation value is used and not updated according to the data whereas the nuisance parameter includes the systematic parameter in the fit and allows its best value to change.

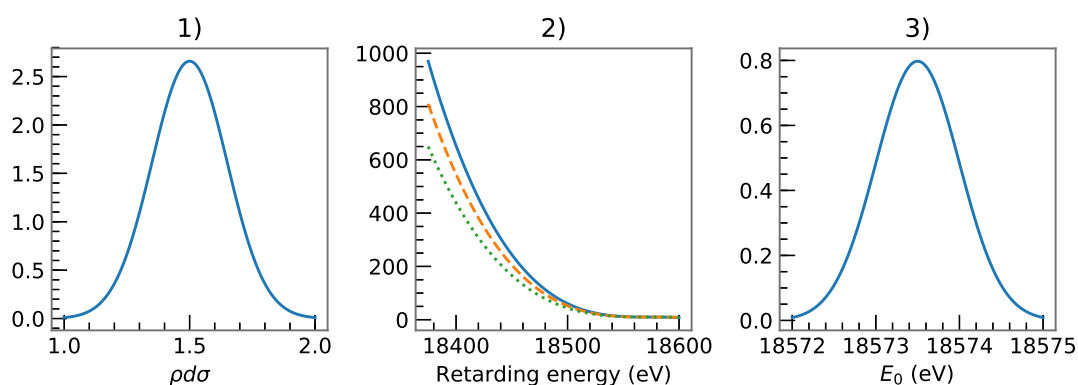


Figure 3.6: Monte Carlo propagation procedure, ordinate in arbitrary units.

- 1) Sampling distribution
- 2) Models with different value of systematic parameters
- 3) Fitted parameter distribution

3.4.3 Covariance Matrix Approach

Within the framework of χ^2 -minimization, another option similar to the full Monte Carlo propagation of uncertainty is available using covariance matrices. In this case, instead of performing a full fit with each drawn systematic parameter, the covariance matrix V_{sys} of the different spectra is calculated. This is done by:

- Retrieving N_{spectra} different model spectra, each with n elements with corresponding rates $\vec{\mu}$, drawing the systematic parameter from a given distribution.
- Calculating the covariance of the rates in the spectra using

$$\text{cov}(\vec{\mu}_i, \vec{\mu}_j) = \frac{1}{N_{\text{spectra}}} \sum_{l=1}^{N_{\text{spectra}}} (\mu_{i,l} - \langle \vec{\mu}_i \rangle)(\mu_{j,l} - \langle \vec{\mu}_j \rangle).$$

Here $\vec{\mu}_i$ is the vector containing all rates of the point i resulting from varying the systematic parameter, $\mu_{i,l}$ is the l^{th} element in the vector and $\langle \vec{\mu}_i \rangle$ is its expectation value.

- Combining the individual covariances to the covariance matrix

$$V_{\text{sys}} = \begin{pmatrix} \text{cov}(\vec{\mu}_0, \vec{\mu}_0) & \text{cov}(\vec{\mu}_0, \vec{\mu}_1) & \cdots & \text{cov}(\vec{\mu}_0, \vec{\mu}_n) \\ \text{cov}(\vec{\mu}_1, \vec{\mu}_0) & \text{cov}(\vec{\mu}_1, \vec{\mu}_1) & \cdots & \text{cov}(\vec{\mu}_1, \vec{\mu}_n) \\ \vdots & \vdots & \ddots & \vdots \\ \text{cov}(\vec{\mu}_n, \vec{\mu}_0) & \text{cov}(\vec{\mu}_n, \vec{\mu}_1) & \cdots & \text{cov}(\vec{\mu}_n, \vec{\mu}_n) \end{pmatrix}.$$

This covariance matrix reflects the uncertainty the systematic effect introduces onto the spectrum and keeps track of the correlation between different data points. It is usable if higher order terms are negligible and the points of the different spectra are distributed by a multi-variate normal distribution.

The calculation of the covariance matrix can be performed independently for different systematic effects k , resulting in multiple matrices $V_{\text{sys},k}$. The combined covariance matrix is then

$$V_{\text{sys}} = \sum_k V_{\text{sys},k} \quad (3.9)$$

where k runs over the different systematic effects. Statistical uncertainty is approximated by the square root of the counts $\sqrt{N_i}$ at each data point i . In the covariance matrix representation, this results in the diagonal matrix

$$V_{\text{stat}} = \begin{pmatrix} N_1 & & \mathbf{0} & \\ & N_2 & & \\ & & \ddots & \\ \mathbf{0} & & & N_n \end{pmatrix} \quad (3.10)$$

where n indicates the total number of points in the data spectrum.

Finally, the total covariance matrix including systematic and statistical uncertainty is retrieved by adding these two components:

$$V_{\text{tot}} = V_{\text{sys}} + V_{\text{stat}}. \quad (3.11)$$

This matrix is then plugged into the χ^2 function which gives:

$$\chi^2(\vec{\mu}; \vec{N}) = (\vec{\mu} - \vec{N})^T V_{\text{tot}}^{-1} (\vec{\mu} - \vec{N}). \quad (3.12)$$

The resulting χ^2 is then minimized as usual.

Advantages of this approach are the possibility to treat systematic effects individually and combine them later, the option to calculate the covariance matrix once and use it for multiple fits and therefore the overall flexibility and speed. Downside is that it relies on two assumptions:

1. As the χ^2 -minimization is used, the data is assumed to follow a Gaussian distribution which is only valid for high model rates μ .
2. The calculation of the covariance matrix implies that the systematic effect varies the data points as if they were drawn from a multi-variate normal distribution.

Chapter 4

New Analysis Tool: *Fitrium*

To efficiently employ the analysis strategies described in chapter 3, a new analysis tool named *Fitrium* (Fit Tritium) was developed within the course of this thesis. It is written entirely in the C++ programming language, utilizes the boost library [26], builds upon the Fitness Studio, a software framework developed by Martin Slezák for fitting models to data by maximum likelihood estimation, and is meant to run on GNU/Linux based operating systems.

Fitrium includes a model of the tritium β -decay and the KATRIN apparatus, an application for Monte Carlo data generation and an application for data fitting as well as various utility functions. This chapter explains the physics components that are contained in the model, the overall design of the code as well as the user interface provided. Additionally a brief overview of the numerical methods is given and a validation of the implemented model is performed.

4.1 Physics Components

The most important effects describing the β -spectrum are included in *Fitrium*. Other less significant effects such as synchrotron radiation and theoretical corrections can be implemented in the future as needed given the existing statistical sensitivity of the KATRIN experiment.

Modelling of the differential β -spectrum is done according to (2.15). The final state distributions are read from text files. Currently included files for the corresponding isotopologues are HT (Saenz), DT (Doss), T₂ (Doss) and T₂ (Saenz) [21, 27].

The response function of the KATRIN experiment described by (2.27) is included in the model. Therefore the analytical expression of the transmission function (2.20), the energy loss function (2.26) and energy-dependent scattering probabilities (2.23, 2.24) are all part of the code.

As an additional correction to the β -spectrum, the Doppler effect described in 2.5.2 is also implemented.

Finally it is worth mentioning that pixel-dependent effects are naturally part of the model. This is described in more detail section 4.2.

4.2 Code Structure

Here an overview of the code structure and the idea behind it is given. An in-depth explanation of the C++ code can be found in appendix C. The complete structure of the code is visualized in figure 4.1.

Basic building block of the *Fitrium* model is the description of the rate expectation of a single pixel of the focal plane detector in the `ModelPixel` class. As each pixel is assigned its own model, parameters varying between pixels can be treated naturally by constructing models with different values for these parameters. To use the different pixel combination methods described in 3.2, the single pixel models are treated accordingly. In case of the uniform fit, the whole detector is treated as if it was a single pixel. Therefore only one `ModelPixel` is required which uses averaged parameter values. In contrast, when performing a single-pixel fit, there is one `ModelPixel` per detector pixel and each of them is treated independently. Finally for the multi-pixel fit there is one `ModelPixel` for each detector pixel, but they share parameters such as the neutrino mass squared.

In *Fitrium* three components make up the rate expectation of a single pixel: a description of the signal rate in the `ModelSignal` class, the `Background` class and the `Detector`. Decoupling these allows changing one part without having to update another and keeping the overall pixel combination structure. Currently the `Background` is a polynomial of order 0 which takes care of the free parameter B .

The `Detector` class handles the detector efficiency and knows about the overall pixel segmentation. This allows proper normalization of the rate depending on whether the model applies to a single pixel as in the single-pixel and multi-pixel fits or to the complete detector in the uniform fit.

In `ModelSignal`, which corresponds to the integrated tritium spectrum, an `IntegratedSpectrum` is combined with the normalization parameter A_S and a `Source` class. It therefore calculates the total signal rate which is expected at the detector.

Task of the `IntegratedSpectrum` class is to integrate an arbitrary differential spectrum over any response function. As the lower integration boundary is $qU + \Delta qU$ (3.5), the ΔqU parameter is handled by the integrated spectrum. Two different integration algorithms are

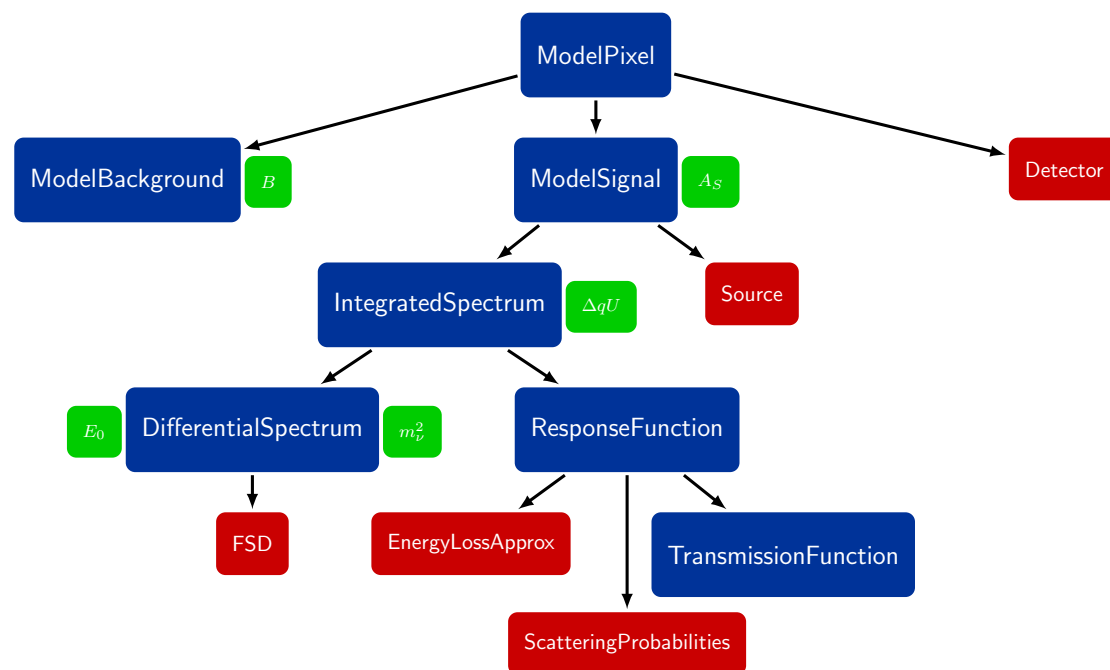


Figure 4.1: Class diagram of models in *Fitrium*. Models are colored in blue, additional classes in red, and parameters in green next to the model which owns them. Models are defined as classes that inherit from the `ModelBase` class described in appendix C.

available. A custom local adaptive integration algorithm using Gauss-Legendre quadrature with Kronrod extension explained in [15, p. 68] and a non-adaptive integration algorithm from the GNU Scientific Library (GSL) [28].

The class `Source` which characterizes the source provides the effective number of tritium atoms by combining column density with the effective source area (2.13) and is able to calculate the solid angle (2.9).

In nominal KATRIN mode, the differential spectrum is the differential tritium spectrum including final states which is implemented according to (2.15). The `FSD` class takes care of reading final state distributions from file and evaluating the sum over all final states

$$\sum_f P_f \cdot \epsilon_f \cdot \sqrt{\epsilon_f^2 - m_\nu^2} \quad (4.1)$$

while the `DifferentialSpectrum` calculates the remaining factors such as the Fermi function and handles the parameters E_0 and m_ν^2 . There are different implementations of the `FSD` class corresponding to the calculations of different theory groups [21, 27] and the three tritium isotopologues HT, DT and T_2 . When reading in the final states of a single isotopologue, for example T_2 , it is also weighted by its abundance in the source therefore ensuring correct normalization.

To allow integration over an arbitrary response function, all response function classes inherit from a virtual base class and must provide the call operator

```
// Pure virtual call operator which must be provided by response functions.  
virtual double operator()(double Ekin_electron, double qU) const = 0;
```

which corresponds to the probability of an electron with kinetic energy $E_{kin_electron}$ to pass the spectrometer with a set retarding energy of qU . When performing tritium measurements, the ResponseFunction class is a combination of three components, EnergyLossApprox, ScatteringProbabilities and TransmissionFunction as described in 2.5.3.

The EnergyLossApprox class calculates the energy loss function according to (2.26) at discrete points and stores the values. A discrete convolution of these values is performed to retrieve the energy loss function for two scatterings. The process of discrete convolutions is repeated iteratively until a user-defined number of scatterings has been considered and the corresponding values have been stored. To calculate the continuous energy loss function for n scatterings, a cubic splines interpolation of the matching saved values is performed.

There are two options for the ScatteringProbabilities class. First of all, there is the simple ScatteringProbabilities representation which calculates the probability to scatter zero to n times at given energy and slow control parameters. Here n is the maximum number of scatterings to be considered. These probabilities are stored and can be retrieved with the GetProbability(int n_scatterings) method. To include the energy dependent scattering cross section (2.24), the ScatteringProbabilitiesApprox class can be used. It calculates the probabilities zero to n for multiple values of the product of column density and inelastic cross section $\rho d\sigma$ and saves these values. To retrieve the scattering probability at any $\rho d\sigma$ value and therefore any $\rho d\sigma(E)$, cubic splines interpolation is used.

Finally, the TransmissionFunction is the implementation of (2.20) including the relativistic correction.

4.3 User Interface

This section gives an overview of the complete user interface of *Fitrium*, showing the different configuration options and tools available to the end-user.

In the KATRIN experiment the processed data required by fitting tools is stored in a *run summary* file. As such it contains information on counts, retarding energies and measuring time as well as various slow control parameters such as the column density ρd . For ease of reading and processing in various programming languages, this *run summary* file is converted to

the HDF5 [29] format within the *Fitrium* framework.

Fitrium provides a command line tool, `fitrium_fit`, which reads the information in the *run summary*, performs a maximum likelihood analysis and writes the fit results and other meta data to an output file which is also in the HDF5 format. Configuration of model and analysis can be done at runtime editing an initialization (`ini`) file and providing command line arguments. Both the configuration file and the command line options are well documented. An overview of the available options is given in the following paragraphs.

Options that can be set in the configuration file include:

- The likelihood type to use which defines the underlying probability distribution function. Currently available is the Poisson distribution, the normal distribution and the normal distribution with covariance matrix to include systematic effects.
- All slow control parameters defining the model such as the column density, the magnetic field values or the detector efficiency. As these can be defined in the run summary file as well, they are treated in a special way which is described later in this section.
- The initial value of the fit parameters such as m_ν^2 or E_0 .
- Other model configurations such as the type of final state distribution, the activation of the Doppler effect and the number of scatterings to consider.
- The differential spectrum and response to use in the integrated spectrum. Currently, in addition to the differential tritium spectrum with one effective neutrino mass squared, a spectrum including an additional neutrino mass eigenstate corresponding to a possible sterile neutrino [30] is available. Options for the response function are the exact response function as derived in (2.27), an interpolated response explained in section 4.4 and the plain transmission function (2.20).
- Numerical and computational settings such as the integration method and precision as well as the number of computing threads.
- The activation of various nuisance parameters and the definition of their Gaussian uncertainty.

In addition, the command line provides options for defining:

- The run summary file(s) to read in and analyse.
- Analysis strategies to use such as the pixel and run combination method.
- The size of the analysis window which defines the retarding energies that are consid-

Table 4.1: Available plots in *Plotrium* with reference to example figure.

| Plot | Example figure |
|--|----------------|
| Spectrum with residuals | 5.2 |
| Parameter evolution over run | 5.3a |
| Pixel map of fit parameter | 5.5a |
| Pixel distribution of fit parameter | 5.7 |
| Parameter distribution from MC propagation | 5.10 |
| Deviance distribution | 5.9 |
| Correlation plot of two fit parameters | E.1 |

ered. This allows excluding ranges of data points from the analysis, for example in case the model may not be valid over the complete spectrum.

As model values can be defined in multiple places, to retrieve them a three step process is used:

1. Read value from *run summary*.
2. If the previous point is not successful, read value from ini file.
3. If this is also not successful, fall back to a default value.

Therefore slow control parameters which are stored in the *run summary*, such as ρd , are automatically applied to the model. Parameters like the starting value of m^2 , which are not included in the *run summary*, start at the second step.

The fit results file written at the end of the analysis contains information on the best fit parameter values with uncertainty and correlations, a data and model spectrum with corresponding residuals for convenient plotting and various information to ensure reproducibility of the analysis. For quick plotting another toolkit, *Plotrium*, has been developed in python. It can read the fit results and create plots in pdf or png format as well as display the plot on screen. Plots currently available are shown in table 4.1.

Another command line tool, *fitrium_gendata*, is used to generate Monte Carlo data in the HDF5 run summary format. Its model is configured using the same initialization file as *fitrium_fit*. The measuring time distribution (MTD) file which defines which fraction of time is spent at specific retarding energies can be set using a command line flag. MTD files are plain text files with two columns, one for the retarding energy and one for the time fraction. The MTD for first tritium measurements, shown in figure 4.2a, and a simple flat time distribution, displayed in 4.2b, is included in the default installation. To add new MTDs, a file in the correct two column format can be stored in the `~/local/share/Fitrium/data/MTD` folder. The total run time which is multiplied with the fraction of measuring time at each

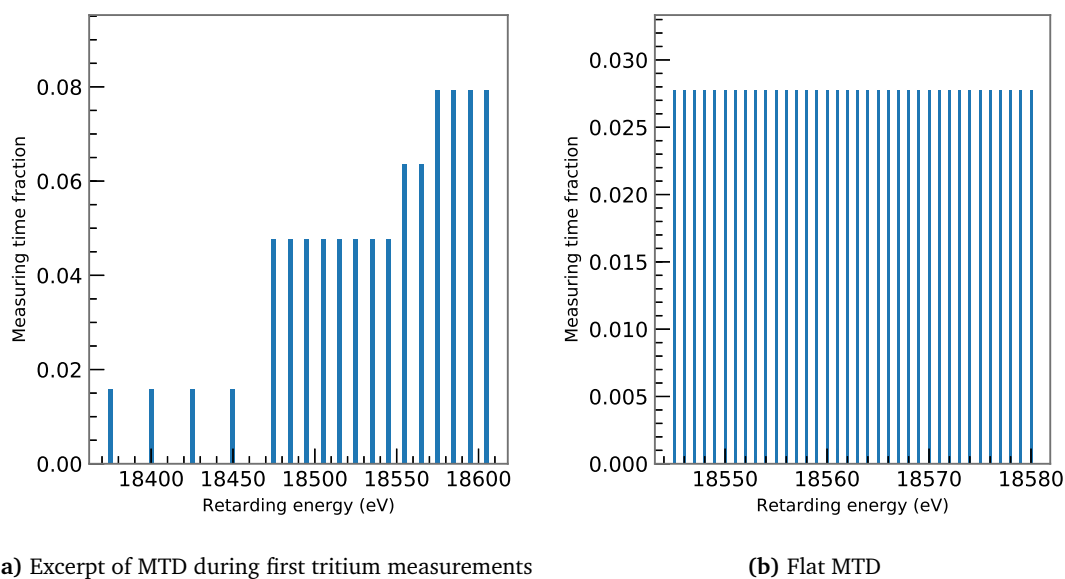


Figure 4.2: Measuring time distributions included in the default *Fitrium* installation. The height of the blue bars indicates which fraction of measuring time is spent at the corresponding retarding energy.

retarding energy, can also be set from the command line. In addition, options to deactivate the Poissonian fluctuation of counts and to smear the retarding energies are provided.

Therefore, for Monte Carlo studies, one can run the following tool-chain:

1. Create one or more run summary files using `fitrium_gendata`. Depending on the study statistical fluctuations may be turned on or off.
2. Analyse the created files with `fitrium_fit`, defining the type of analysis, for example the pixel combination method, at runtime.
3. Visualize the fit results using *Plotrium* or read in the created HDF5 fit results file with a custom script.

The complete study can be performed without having to touch the source code and with multiple configurations available in the initialization file and the command line. When analysing real data, the first step is replaced by retrieving the appropriate HDF5 run summary file. A summary of the user interface and the various tools is shown in figure 4.3.

As an additional aid to the user, a logging infrastructure which allows defining the log level at run time is provided. The default log level, *info*, gives information on the current status of the program. An example output for `fitrium_gendata` is shown in figure 4.4. Much

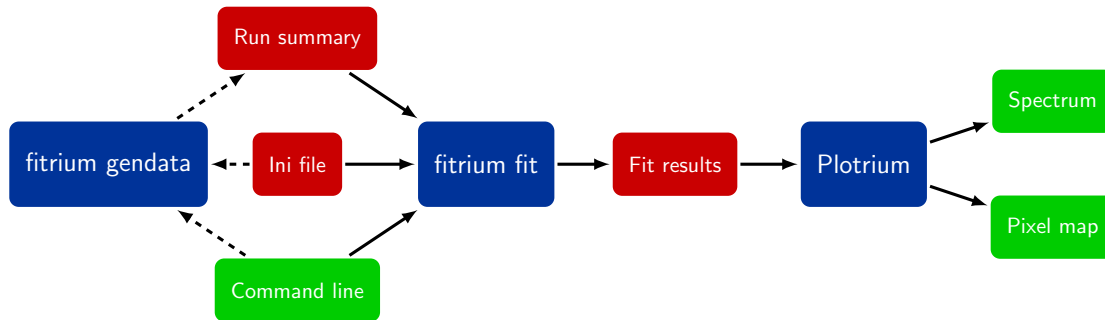


Figure 4.3: Overview of user interface of *Fitrium*. Files are colored in red, developed tools in blue and others in green. *fitrium_fit* processes the input, performs the analysis and writes fit results to file while *Plotrium* is used to create standard plots. It is possible to generate MC run summary files using *fitrium_gendata*.

```

[fitrium] [ INFO] [000.001] Generating MC data
[fitrium] [ INFO] [000.402] Preparing response cache, this may take a while...
[fitrium] [ INFO] [000.408] Wrote MC data to './master_thesis_demo.h5'
[fitrium] [ INFO] [000.409] Done
  
```

Figure 4.4: Example log output of *fitrium_gendata* at log level *info*.

more information can be retrieved when the level is set to *debug* or even *trace* which allows back-tracking problems. If less output is wished, the options *warning*, *error* and *fatal* can be selected.

4.4 Numerical Methods

A major challenge of the KATRIN analysis is the combination of a computationally expensive model calculation with many free parameters. Therefore, the following means to speed up the calculations have been implemented in *Fitrium*.

Multi-Threading

To make use of modern multi-core and multi-thread infrastructures, the model evaluation in *Fitrium* is thread-safe. This allows parallelizing the calculation of the likelihood product (3.3) where the model must be evaluated once per factor. In addition, parallelization is used when calculating the scattering probabilities for different $\rho d\sigma$ values and for preparing the response cache which is explained next.

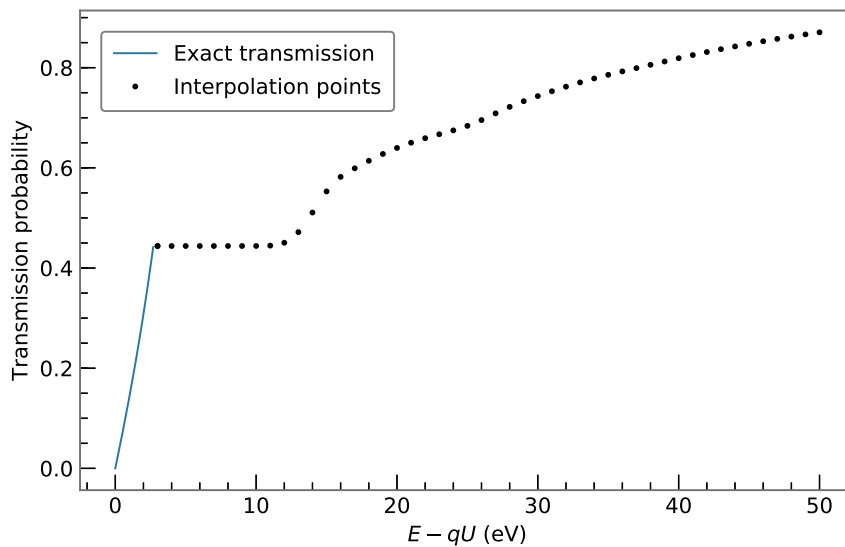


Figure 4.5: Scheme of response function interpolation. The transmission step is always calculated exactly while the rest of the response function is interpolated using cubic splines.

Response Cache

As the response function (2.27) is very expensive to calculate, an additional class was introduced to cache and interpolate the response function. The response function is evaluated at finely spaced discrete points upon construction and cubic splines interpolation is used to approximate the response function between these points. The spacing depends on the size of the analysis interval, typical values are between 0.1 eV to 1.0 eV. As calculating these points is expensive, it can take up to a few minutes, the points are stored in an HDF5 file `~/.cache/Fitrium/response.h5` so they can be re-used in further analyses.

The transmission step at the beginning of the response function must be known very well for neutrino mass analysis. Therefore interpolating it is not feasible and this step is always calculated exactly. This is depicted in figure 4.5.

Interpolating the response function is a large performance improvement, as it leads to a speed up of a simple fit of over an order of magnitude. Downside is that it does not allow fitting parameters that impact the response function like the column density or the magnetic fields. This makes the nuisance parameter method impossible in combination with the approximated response.

Explicit Derivatives

Many algorithms for numerical optimization make use of gradient information to efficiently

find the minimum of a function. Numerical derivatives, which are often used by these gradient-based algorithms, amplify noise and are expensive to calculate as they require multiple model evaluations. To avoid these problems, the derivatives are passed in a semi-analytical way to the minimizer by *Fitrium*.

The derivatives are implemented analytically in the class in which they appear and the numerical value of the derivative is then passed through the remaining steps of the model evaluation. To clarify this procedure let us consider the derivative by the neutrino mass squared m_ν^2 .

The neutrino mass squared appears in the final states sum of the differential spectrum (2.15), so this is where the derivative must be calculated:

$$\frac{d}{dm_\nu^2} (\epsilon_f \sqrt{\epsilon_f^2 - m_\nu^2}) = \frac{-\epsilon_f}{2\sqrt{\epsilon_f^2 - m_\nu^2}}. \quad (4.2)$$

This derivative value can be calculated and then plugged into the final states sum. The updated value of the sum is now passed into the differential spectrum, then into the integrated spectrum and finally to the signal and pixel model. To modify as few lines of code as possible, the evaluation functions are templated. Returning to the example of the neutrino mass squared, the evaluate method of the differential spectrum is templated in the type of final states kinetic term. In model evaluation, the standard KineticTerm function is passed to the evaluate function. To retrieve the derivative with respect to m_ν^2 , KineticTermMnu2Derivative is passed instead. The corresponding code fragments are shown below.

```
// Templated evaluation of differential spectrum to allow easy replacing of
// the different types of final state sums
template <typename FSDFunc>
double DifferentialSpectrum::Evaluate(const DataPointBase &point,
                                     FSDFunc &fsd) const;
...
// Regular kinetic term of final states for standard evaluation
inline double KineticTerm(double eps, double mnu2)
{
    return eps * sqrt(eps * eps - mnu2);
}
// Neutrino mass squared derivative
inline double KineticTermMnu2Derivative(double eps, double mnu2)
{
    return -0.5 * eps / sqrt(eps * eps - mnu2);
}
```

These so called explicit derivatives increase the numerical precision of the derivative by sev-

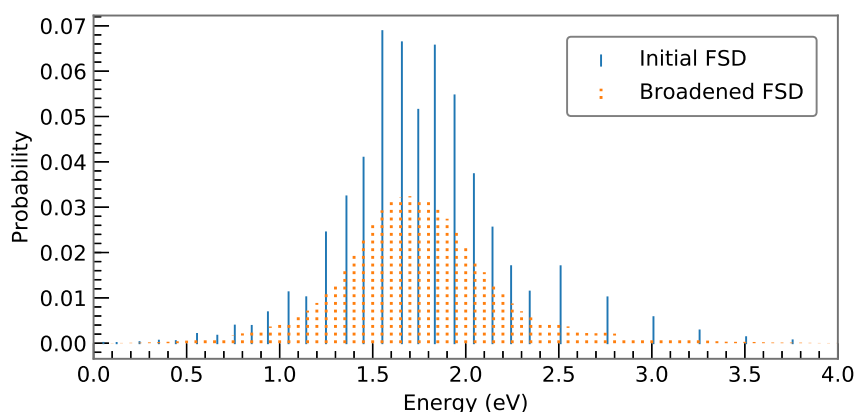


Figure 4.6: Emulation of Doppler broadening in final state distribution. The initial FSD (blue) is transformed to a broader distribution with more states (orange).

eral orders of magnitude and therefore greatly help a gradient-based minimizer. In addition, as the model is only evaluated once per derivative instead of multiple times, a significant speed-up is achieved.

Emulation of Doppler Broadening in FSD

Doppler broadening is described by the convolution of the differential spectrum with a broadening kernel (2.16). As the convolution involves an additional integral, it is very expensive to evaluate. To avoid this integration, *Fitrium* emulates the Doppler broadening in the final states distribution.

This is done by replacing each discrete final state with energy V_f and probability P_f with a Gaussian

$$g_f(E) = \frac{P_f}{\sqrt{2\pi}\sigma_E} \exp\left(-\frac{(E - V_f)^2}{2\sigma_E^2}\right) \quad (4.3)$$

with mean V_f , width σ_E and normalization P_f . This results in a continuous final state function F_{cont} given by the sum over all Gaussian distributions

$$F_{\text{cont}}(E) = \sum_f g_f(E). \quad (4.4)$$

To retrieve an updated, broadened, final state distribution, F_{cont} is then re-binned. This new final state distribution is then used when evaluating the final states sum in the differential spectrum 2.15. The effect on the final state distribution is shown in figure 4.6.

Table 4.2: Comparison of *SSC* input values and *Fitrium* fit results.

| Parameter | Input value | Fit result |
|-----------|----------------------|---------------------------------|
| m_ν^2 | 0.42 eV ² | 0.39 ± 0.05 eV ² |
| E_0 | 18 575 eV | $18\,575.050 \pm 0.004$ eV |
| A_S | 1.0 | $0.999\,36 \pm 0.000\,33$ |
| B | 0.287 cps | 0.287 ± 0.003 cps |

4.5 Validation

To validate the newly developed model, it was cross-checked against the independently developed KATRIN model *SSC* (Source and Spectrum Calculation) [31, p. 85]. In a first step, the numerical values of different components were compared. The components tested include the differential spectrum, the energy loss function, the transmission function, the scattering probabilities and the integrated spectrum. Other than negligible differences occurring from different numerical methods and the use of other references for the values of physical constants, the two models agreed.

For further probing of this agreement at the sensitivity of KATRIN, three years of KATRIN data taking was generated using *SSC* as the underlying model and analysed with *Fitrium*. The tool to create the data file was developed over the course of this thesis and is briefly described in appendix D.

Input values and the retrieved fit results are summarized in table 4.2. m_ν^2 and B were recovered within uncertainty while E_0 and A_S are very close on absolute scale but differ slightly due to for example the different references for the values of physical constants. Overall the two models match very well and thus the developed *Fitrium* model passed the validation test.

Chapter 5

Analysis of First Tritium Data

The KATRIN experiment took first tritium data from May 18 to May 19, referred to as *very first tritium* (VFT) and from June 5 to June 20 referred to as *first tritium* (FT). The goal of these measurements was to commission the full KATRIN system with 1 % of the nominal activity and to demonstrate a global system stability on the 0.1 % level. In addition it allows to study the β -spectrum for systematic effects and to test the analysis strategies.

During the very first tritium campaign a known gas mix with tritium was injected from a prepared cylinder leading to rather unstable slow control parameters, especially to a declining column density over time. During the first tritium measurements the full KATRIN loop system was available and therefore the slow control parameters were more stable. An overview of slow control parameters during the first tritium campaigns can be found in appendix A.

If not mentioned otherwise, the two outer rings of the FPD and pixels 100, 112 and 123 are excluded from the analysis. “The outer two pixel rings show a decreased rate indicating the flux tube boundary. A slight misalignment of the flux tube is noticeable at the bottom left border of the FPD...” [32, p. 24]. Pixels 100, 112 and 123 were shadowed by the forward beam monitor¹.

As the statistics of these measurements is low compared to the final KATRIN analysis, decoupling the endpoint E_0 from work function effects ΔqU is not possible. Therefore for the following analysis an effective endpoint $E_{0,\text{eff}} = E_0 + \Delta qU$ which absorbs these work function effects into the absolute endpoint value is used. The uncertainty of the work function difference between WGTS and main spectrometer is on the order of $\Delta qU \approx \pm 0.5 \text{ eV}$ and is a systematic bias of the effective endpoint compared to the true value.

¹The forward beam monitor (FBM) is a detector used to monitor the incoming electron flux before the KATRIN spectrometers to check rate stability [33].

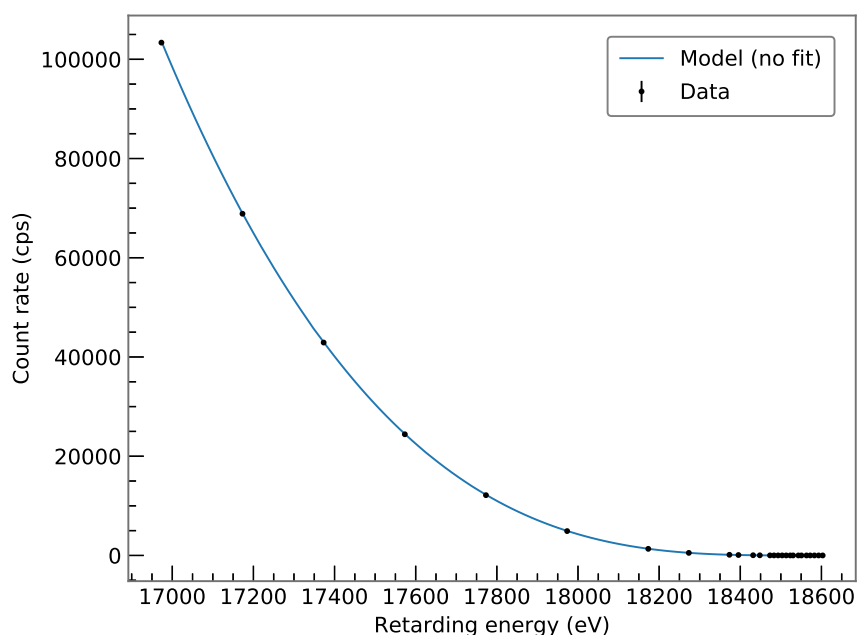


Figure 5.1: Overlay of *Fitrium* model prediction and KATRIN VFT data (run 40263). The model matches the data within 0.3%.

5.1 Initial Comparison of Model and Data

As an initial comparison of the developed model to the data, the model prediction is overlaid with the spectral data of a run of the VFT campaign without performing any fit. As shown in figure 5.1 the model expectation provides agreement with the data within 0.3% in the complete energy range of 1.6 keV below the endpoint.

As next step *Fitrium* is used to fit the model to the data. At first, a uniform fit (all pixels combined as described in 3.2.1) of the data with three free parameters, effective endpoint of the tritium spectrum $E_{0,\text{eff}}$, signal normalization A_S and background rate B is performed. The fit results for the full 1.6 keV range as well as for a smaller 400 eV range below E_0 are shown in figure 5.2. The residuals show no structure and the reduced deviances of $D_{\text{red}} = 0.95$ (17 dof) and $D_{\text{red}} = 1.0$ (23 dof) are in good agreement with the expectation of 1.0^2 .

²The deviance D is a goodness-of-fit statistic generalizing the idea of the χ^2 statistic to arbitrary likelihoods. The reduced deviance is defined as $D_{\text{red}} = D/\text{ndof}$ with the number of degrees of freedom ndof . Asymptotically the deviance follows the χ^2 -distribution with $n-k$ degrees of freedom, where n is the number of observations and k is the number of free parameters in the model. Thus, in such a case, the expected value of D/ndof is one.

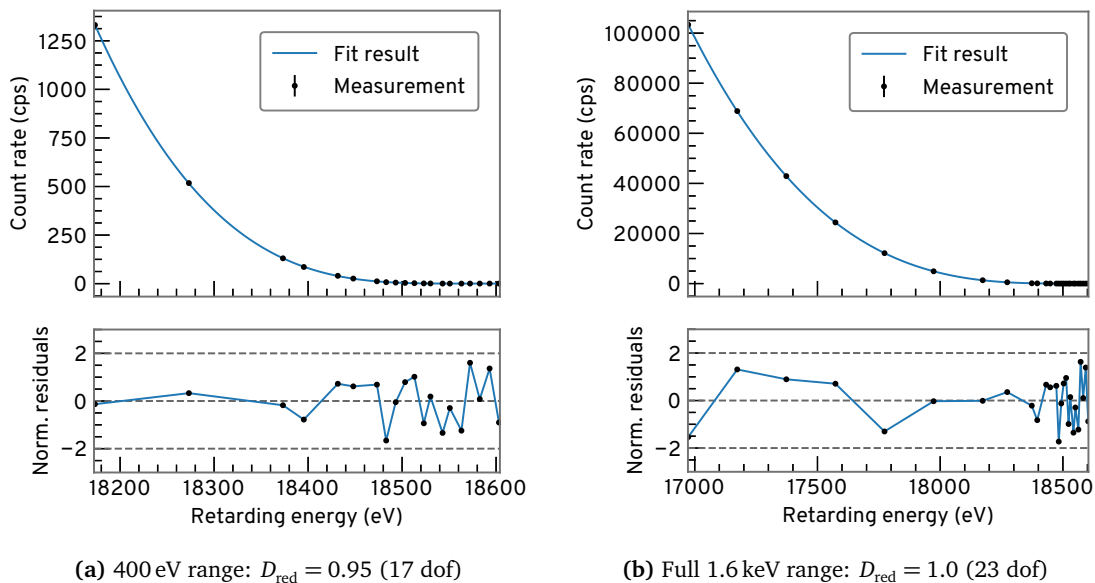


Figure 5.2: Initial uniform fit of KATRIN VFT integral spectrum (run 40263).

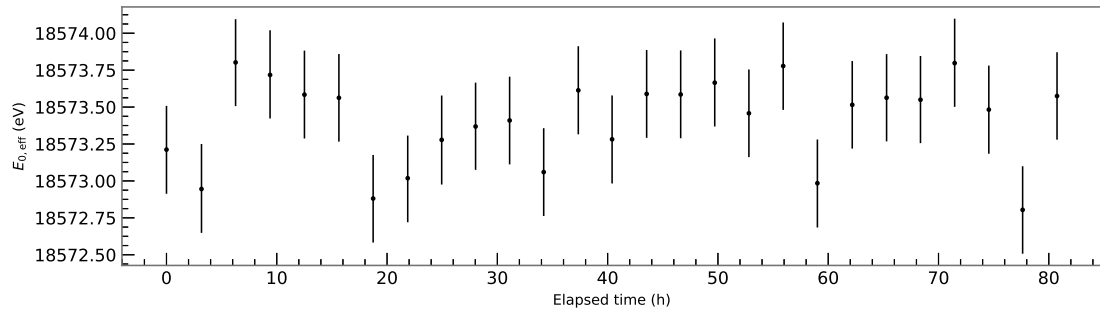
5.2 Parameter Stability over Time

To check the overall stability of the KATRIN system a set of three hour runs of the first tritium campaign is analysed using a uniform fit in the 400 eV range considering only statistical uncertainty. The evolution of the three fit parameters, effective endpoint, signal normalization and background, is displayed in figure 5.3. As one can see in table 5.1, effective endpoint and background are stable within statistical fluctuations. The signal normalization fluctuates more as it is affected directly by many different parameters, for example the column density ρd and the number of tritium atoms N_T . Thus systematic effects must be taken into account to explain this fluctuation.

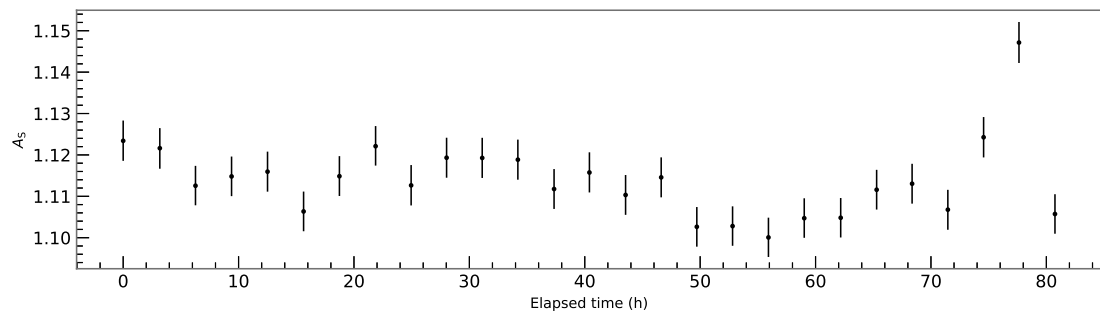
The deviance distribution of these 27 uniform fits is shown in figure 5.4. It matches the expected χ^2 -distribution.

Table 5.1: Goodness of fit of a constant to parameter evolution shown in figure 5.3.

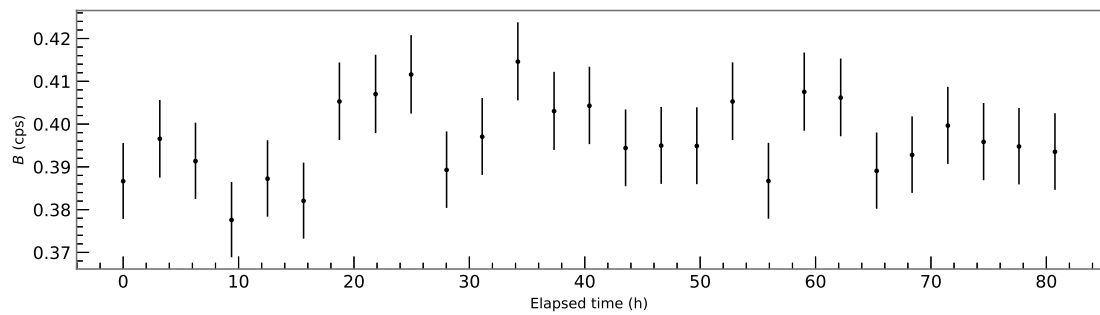
| Parameter | Deviance | ndof | p -value |
|--------------------|----------|------|------------|
| $E_{0,\text{eff}}$ | 25.41 | 26 | 0.49 |
| B | 26.74 | 26 | 0.42 |
| A_S | 98.33 | 26 | 0.00 |



(a) Effective endpoint evolution: $E_{0,\text{eff}} = 18573.410 \pm 0.056 \text{ eV}$, $D_{\text{red}}^{\text{linefit}} = 0.98$ (26 dof)



(b) Normalization evolution: $A_s = 1.1140 \pm 0.0018$, $D_{\text{red}}^{\text{linefit}} = 3.78$ (26 dof)



(c) Background evolution: $B = 0.3966 \pm 0.0018 \text{ cps}$, $D_{\text{red}}^{\text{linefit}} = 1.02$ (26 dof)

Figure 5.3: Parameter evolution during FT measurements, runs 40 667 to 40 693, uniform fit. The reduced deviances correspond to the result of fitting a constant to the data. Effective endpoint and background are stable within statistical fluctuations while the normalization fluctuates more due to systematic effects.

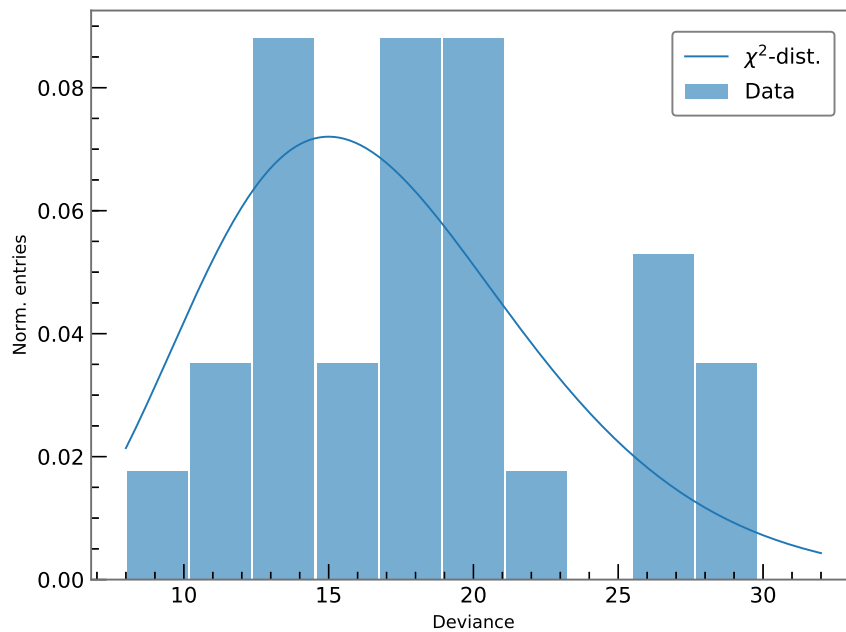


Figure 5.4: Deviance distribution of the 27 uniform fits of runs 40667 to 40693 compared to the expected χ^2 -distribution.

5.3 Parameter Distribution over the Focal Plane Detector

To check for spatial inhomogeneities, the data of runs 40667 to 40693 is appended as explained in 3.3.2 and each pixel is fit individually. The resulting parameter distribution is displayed over the KATRIN detector pixel map in figure 5.5.

The effective endpoint map 5.5a and the normalization map 5.5b show no structure. In contrast the background map shows a clear radial and azimuthal dependence as seen in 5.5c. The pattern is compatible with the one obtained in an earlier background-only measurement [34, p. 79].

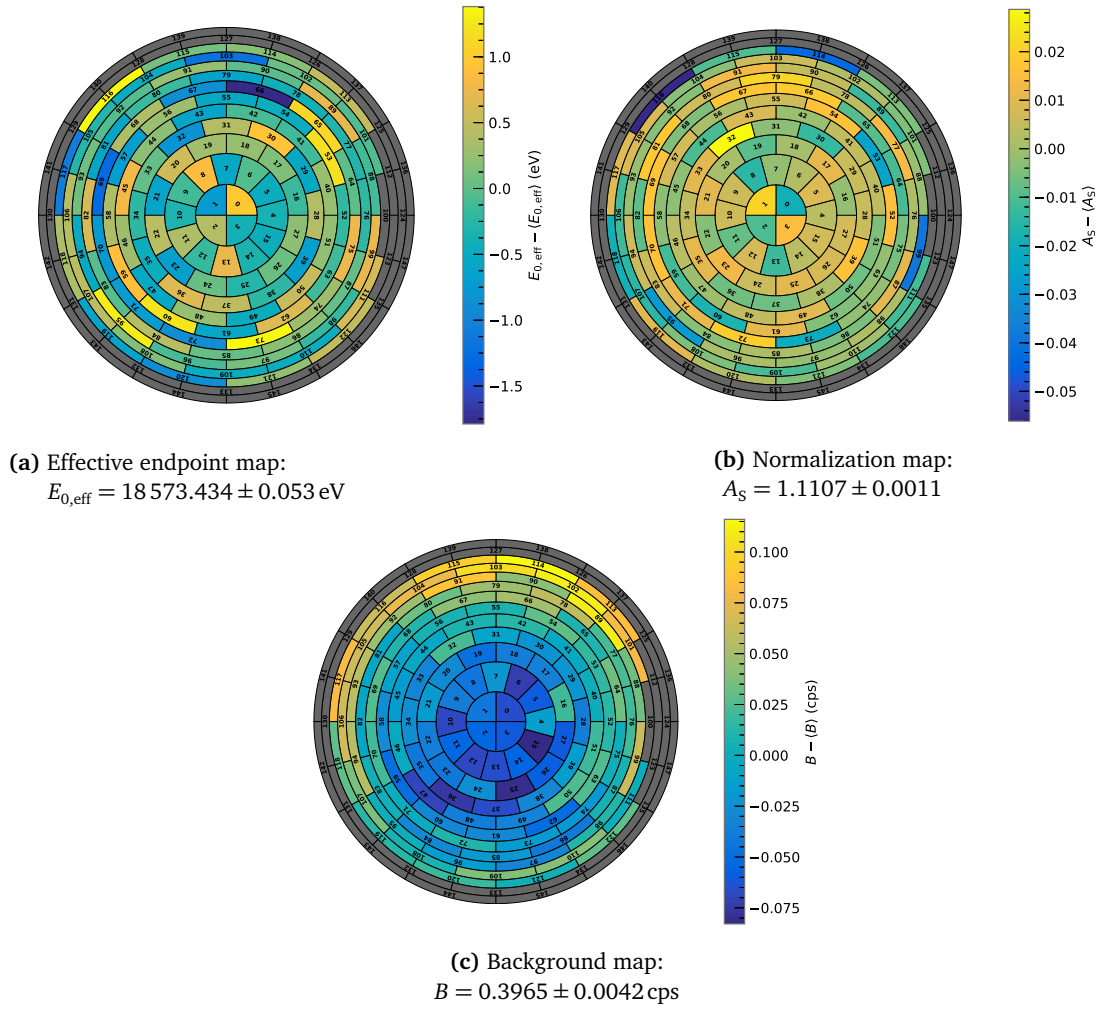


Figure 5.5: Distribution of fit parameter differences from their mean values over the KATRIN FPD, runs 40 667 to 40 693, single-pixel fit, runs appended. Effective endpoint and normalization show no structure whereas the background has a clear radial and azimuthal dependence.

5.4 Comparison of Analysis Strategies

The analysis strategies introduced in chapter 3 are now applied to first tritium data and compared using the value of the effective endpoint $E_{0,\text{eff}}$ as physics parameter of interest for comparison. The 400 eV energy range is always used.

5.4.1 Pixel Combination

To compare different pixel combination methods all runs from 40 667 to 40 693 are analysed independently with the three different approaches using statistical uncertainty only. The fit result for the effective endpoint is summarized in table 5.2 for run 40 667 as an example.

The values for the effective endpoint are equal within uncertainty and the uncertainties are comparable. This also holds for the other runs analysed. To compare the goodness-of-fit of the different methods, the reduced deviance and the p -values for all 27 runs are shown in figure 5.6. On the one hand the average p -value of the uniform fit of 0.40 is closer to the expectation of 0.5 than the one of the single- (0.10) and multi-pixel (0.12) fit respectively. On the other hand the reduced deviances of the uniform fit have a much larger spread and the average value is larger than the one of the single-/multi-pixel fit. This can be explained by the fact that the number of degrees of freedom is much larger for the single- (2057 dof) and multi-pixel (2177 dof) fit which leads to a very narrow χ^2 -distribution. Therefore slight divergences from the expectation of $D_{\text{red}} = 1.0$ result in a low p -value.

The fact that the three different methods lead to very comparable results leads to two independent conclusions. As the uniform fit, which makes use of an averaged model, leads to the same results as the single-/multi-pixel fits, the small model differences between the individual pixels have no significant impact at the current statistical sensitivity. Furthermore, since the single-pixel fit, which uses mean and error on the mean to combine pixels, agrees with the multi-pixel fit, the distribution of the individual fit results over pixel is approximately Gaussian, as shown in figure 5.7. As KATRIN takes more data, these two statements may no longer hold.

Table 5.2: Fit result summary of different pixel combination strategies for run 40 667.

| | $E_{0,\text{eff}}$ (eV) | Deviance | ndof | p -value |
|--------------|-------------------------|----------|------|------------|
| Uniform | $18\,573.21 \pm 0.30$ | 11.44 | 17 | 0.83 |
| Single-pixel | $18\,573.11 \pm 0.27$ | 2159 | 2057 | 0.06 |
| Multi-pixel | $18\,573.20 \pm 0.32$ | 2259 | 2177 | 0.11 |

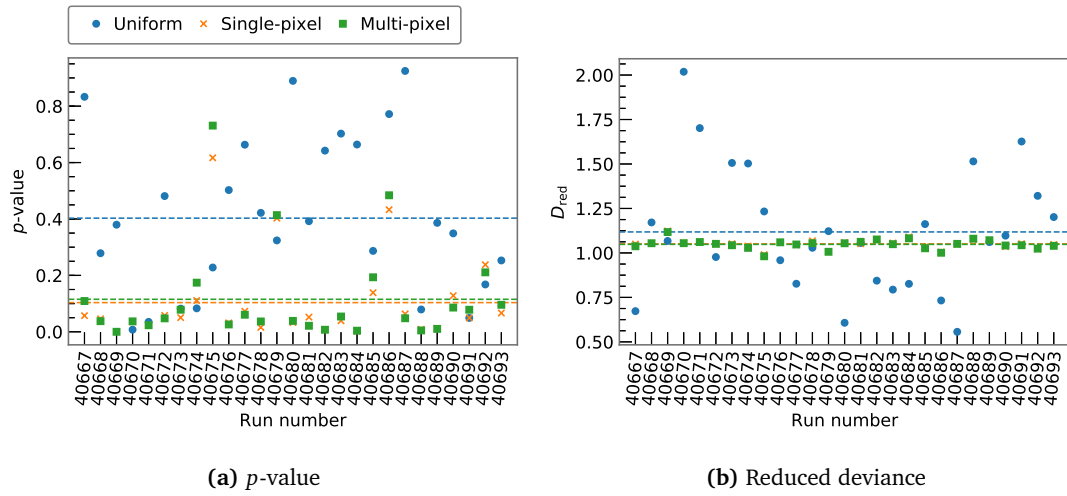


Figure 5.6: p -value and reduced deviance of different pixel combination strategies for runs 40 667 to 40 693. The points correspond to the values of a single run. The dashed line represents the mean value.

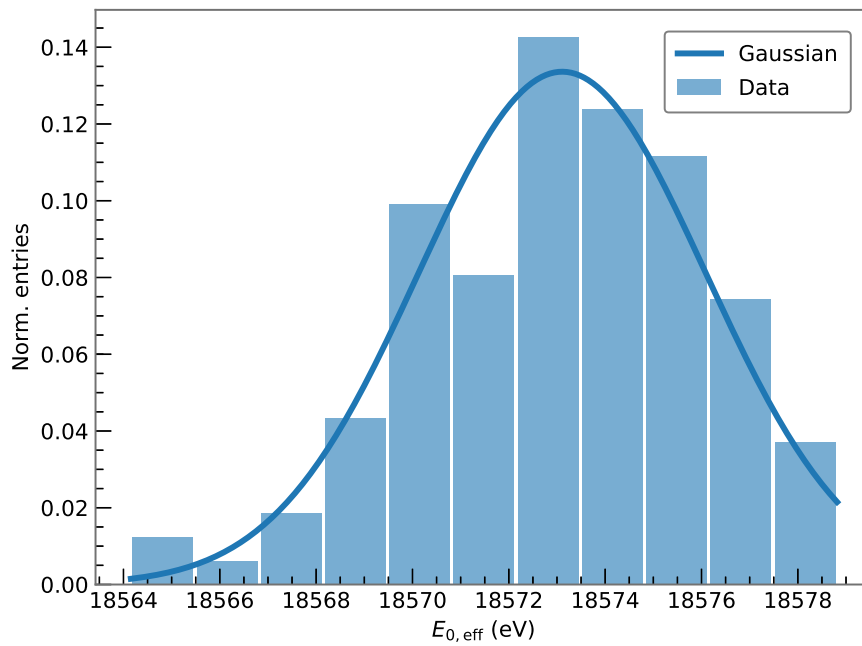


Figure 5.7: Distribution of effective endpoints for single-pixel fits in run 40 667. The fit results follow the Gaussian distribution.

5.4.2 Run Combination

Here run stacking and run appending explained in 3.3.1 and 3.3.2 is compared by combining runs 40 667 to 40 693 using statistical uncertainty only. As a first step, the spectra and fit results resulting from a uniform fit are compared in figure 5.8 and table 5.3 respectively.

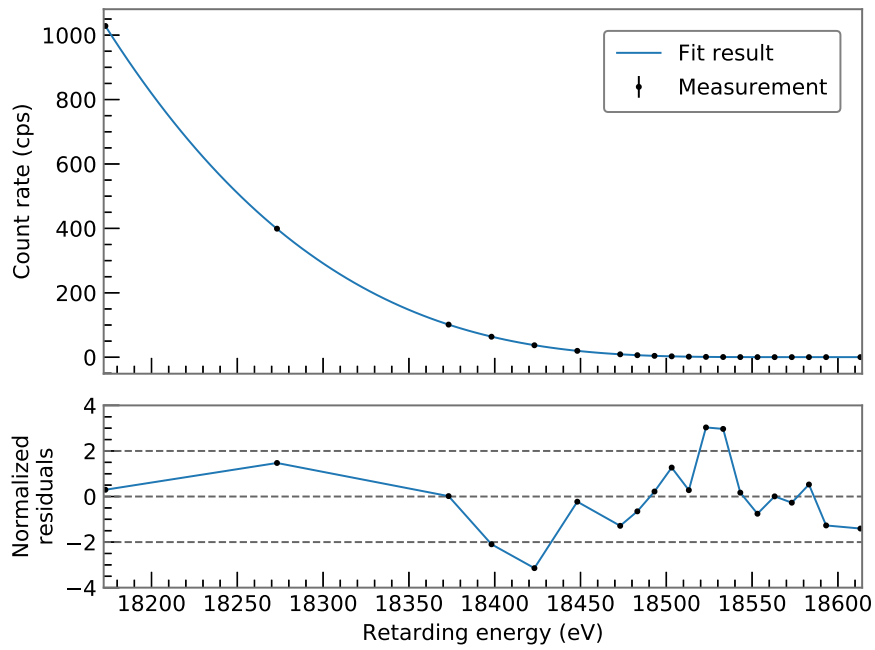
Table 5.3: Results of different run combination strategies for uniform fit of runs 40 667 to 40 693.

| | $E_{0,\text{eff}}$ (eV) | Deviance | ndof | p -value |
|----------|-------------------------|----------|------|------------|
| Stacked | $18\,573.41 \pm 0.06$ | 42.9 | 17 | 0.0004 |
| Appended | $18\,573.41 \pm 0.06$ | 589.5 | 537 | 0.06 |

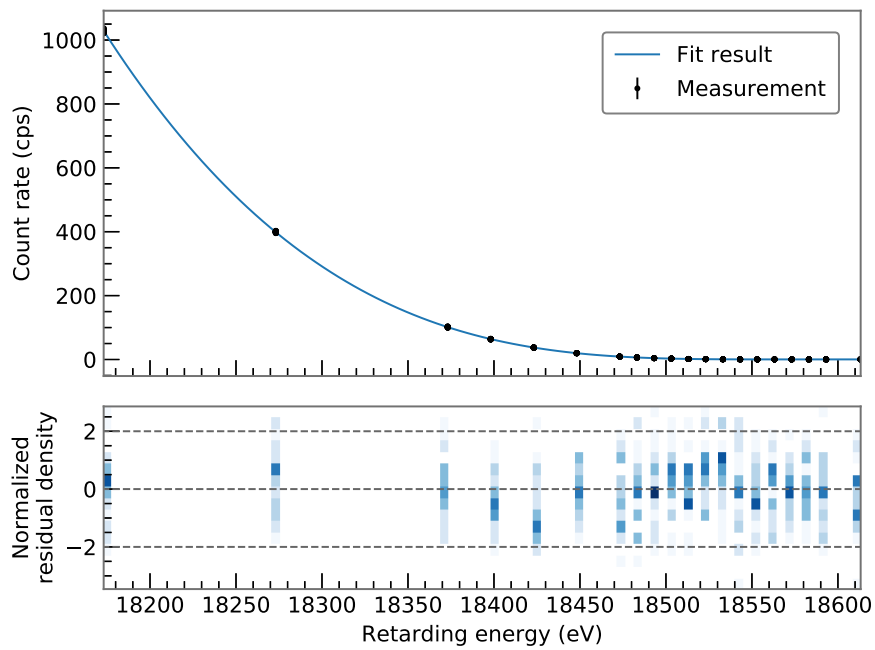
Both residuals show no clear structure and a comparable tendency. The effective endpoint value and uncertainty retrieved by stacking and appending is identical but in this case the model description of the stacked spectrum can be rejected at the $3\text{-}\sigma$ level when not including systematic effects.

As a next step, the single-pixel fit is used to be able to compare the deviance distributions of the two run combination approaches which are displayed in figure 5.9. As one can see, in the case of stacking the χ^2 -distribution is reproduced while when appending the fitted deviances are shifted slightly to larger values. Similar to the single- and multi-pixel fit, when appending runs, the number of degrees of freedom is very large and small differences between model and data show drastically.

Overall, there is no significant difference between run stacking and appending at the sensitivity of first tritium data. Further investigation of their effect for neutrino mass measurements will be done.



(a) Stacked: $E_{0,\text{eff}} = 18573.41 \pm 0.06 \text{ eV}$, $D_{\text{red}} = 2.52$ (17 dof)



(b) Appended: $E_{0,\text{eff}} = 18573.41 \pm 0.06 \text{ eV}$, $D_{\text{red}} = 1.09$ (537 dof)

Figure 5.8: Spectrum and residuals for uniform fit of runs 40 667 to 40 693.

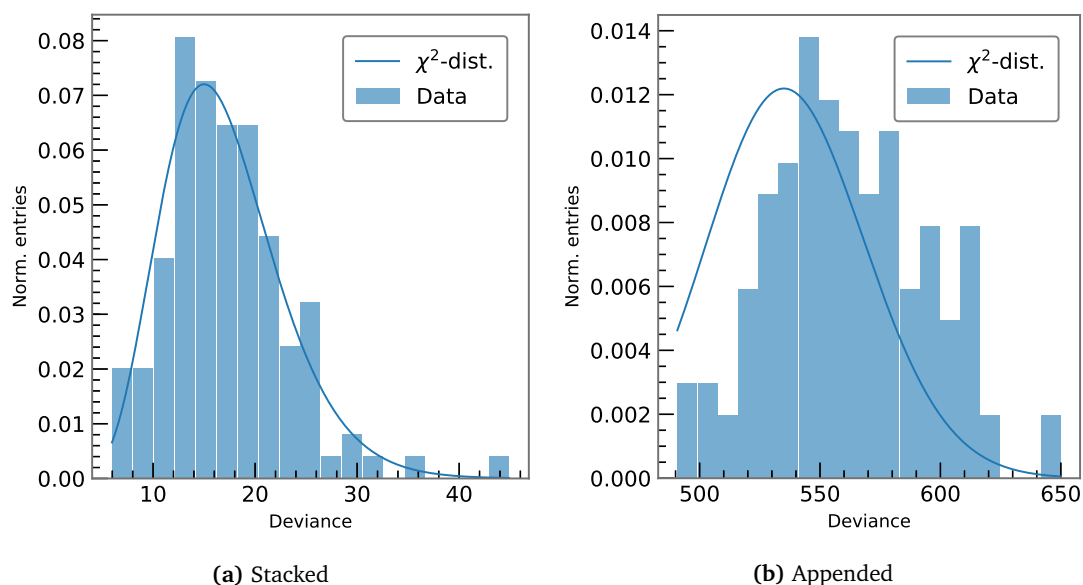


Figure 5.9: Deviance distribution for single-pixel fit of runs 40 667 to 40 693. In the stacked case the data matches the χ^2 -distribution while the data is shifted to slightly larger values when appending.

5.4.3 Treatment of Systematic Effects

Run 40 667 is analysed using the uniform fit with the three different approaches for treatment of systematic effects for comparison. A single systematic parameter, the column density ρd with uncertainty 5%, is considered for simplicity. As a reminder, the result for the corresponding fit with statistical uncertainty only was $E_{0,\text{eff}} = 18\,573.21 \pm 0.30$ eV. The MC propagation method leads to the effective endpoint distribution shown in 5.10 with a width of $\sigma_{\text{sys}} = 0.46$ eV and hence a total uncertainty of $\sigma_{\text{total}} = 0.55$ eV when adding in squares. All results are summarized in table 5.4.

Table 5.4: Results of different systematic treatments for uniform fit of run 40 667. The results for the effective endpoint agree within uncertainty. All uncertainties are between 0.5 eV to 0.55 eV. When using the covariance matrix approach, the goodness-of-fit is described by the χ^2 . In the other cases the deviance is used.

| | $E_{0,\text{eff}}$ (eV) | Deviance / χ^2 | ndof | p -value |
|--------------------|-------------------------|---------------------|------|------------|
| Statistical only | $18\,573.21 \pm 0.30$ | 11.44 | 17 | 0.83 |
| MC propagation | $18\,573.21 \pm 0.55$ | 11.30 | 17 | 0.84 |
| Nuisance parameter | $18\,573.23 \pm 0.52$ | 11.29 | 17 | 0.84 |
| Covariance matrix | $18\,573.17 \pm 0.52$ | 11.46 | 17 | 0.83 |

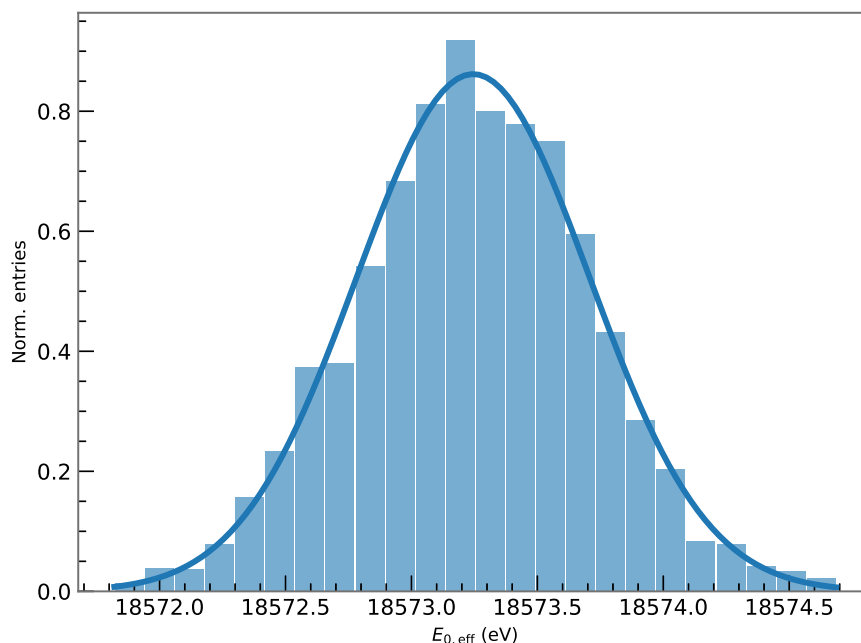


Figure 5.10: Effective endpoint distribution from Monte Carlo propagation compared to a Gaussian. The distribution matches the normal distribution with $E_{0,\text{eff}} = 18573.24 \pm 0.46$ eV.

In all three cases, including the systematic uncertainty on the column density increases the uncertainty on the effective endpoint from 0.30 eV to around 0.5 eV to 0.55 eV. The results for the effective endpoint all agree within uncertainty. Thus, in this case, all three approaches were successfully applied to the data. As the nuisance parameter method and the covariance matrix approach provide the convenience of not having to perform several thousands of fits, they are preferred over the full Monte Carlo propagation of uncertainty. As the covariance matrix is being studied extensively by another team in the KATRIN experiment [35], the focus of the following analyses will be on the pull term method.

5.5 Analysis with Major Systematic Effects

After comparing the various analysis strategies, a complete analysis with major systematic effects is performed for runs 40 667 to 40 693. As the sophisticated pixel combination methods do not have an impact on the analysis at the sensitivity of first tritium data, the uniform fit is used.

Only Nuisance Parameter

In a first step, all runs are appended and the systematic uncertainties are all treated with the nuisance parameter approach. The systematic effects considered are:

- 2 % on the magnetic field in the source B_S
- 2 % on the maximum magnetic field B_{\max}
- 2 % on the magnetic minimum magnetic field B_{\min}
- 5 % on the column density ρd
- 2 % on the inelastic cross section σ_{inel}
- 3 % on the FSD onset parameter F

with the FSD onset parameter F which describes the ratio between rovibrational ground state and electronic excited states. The fit results are summarized in table 5.5. Compared to the appended fit without systematics, the uncertainty on the effective endpoint increases from 0.06 eV to 0.20 eV and the p -value improves from 0.06 to 0.12.

Nuisance Parameter and Covariance Matrix

As this analysis did not include the uncertainty on the activity fluctuation due to fluctuation of the DT concentration in the source within one run and this uncertainty is difficult to parametrize with a pull-term, in a second step the nuisance parameter and covariance matrix method are applied simultaneously. In this case, the runs have to be stacked to reach a large enough number of counts to use the χ^2 -minimization. The systematic uncertainties are treated as following:

- pull term on $\rho d \sigma_{inel}$ with uncertainty $\sqrt{5\%^2 + 2\%^2} = 5.39\%$,
- pull term on F with uncertainty 3 %,
- one covariance matrix including the uncertainties on the three magnetic fields, namely 2 % on B_S , 2 % on B_{\max} and 2 % on B_{\min}
- and one covariance matrix including the 0.1 % uncertainty on the activity fluctuation within one run.

The result of this analysis is also displayed in table 5.5. Including systematic effects significantly improves the stacked fit, the deviance reduces from 42.9 to 20.06 which corresponds to an increased p -value from 0.0004 to 0.27. The uncertainty on the endpoint was raised from 0.06 eV to 0.24 eV.

Table 5.5: Fit results for uniform fit of runs 40 667 to 40 693 including systematic effects. In case of only using nuisance parameters, the runs were appended whereas when adding the covariance matrix the runs were stacked. When using the covariance matrix approach, the goodness-of-fit is described by the χ^2 . In the other case the deviance is used.

| | $E_{0,\text{eff}}$ (eV) | Deviance / χ^2 | ndof | p -value |
|------------------------------------|-------------------------|---------------------|------|------------|
| Nuisance parameter | $18\,573.88 \pm 0.20$ | 575 | 537 | 0.12 |
| Nuisance parameter and cov. matrix | $18\,574.33 \pm 0.24$ | 20.06 | 17 | 0.27 |

In both analyses the uncertainty on the effective endpoint is increased and the goodness-of-fit is improved compared to the statistics-only analysis. This is expected when including additional systematic uncertainty. On top of that a tendency to increase the effective endpoint value when adding systematic effects is observable. With statistical uncertainty only, $E_{0,\text{eff}} = 18\,573.41$ eV, when adding multiple systematic effects with the nuisance parameter approach it increases to $E_{0,\text{eff}} = 18\,573.88$ eV and the addition of the activity fluctuation as systematic effects leads to another raise to $18\,574.33$ eV. Overall, both methods are in good agreement.

Additional systematic effects which were not included in this analysis are uncertainties on the parameters of the energy loss function (2.26). Also, the uncertainty on the FSD will be refined in the future. For this work, the FSD onset is treated with an overestimated uncertainty of 3% to compensate for non-considered uncertainties of the individual excitation probabilities.

5.6 Summary of Fit Results

Table 5.6 summarizes the results for the effective endpoint of the different analysis techniques for quick reference. The table is visualized in figure 5.11.

Table 5.6: Overview of fit results from different analysis strategies. The appended analysis including systematics corresponds to the one in 5.4.3 with only nuisance parameters whereas the stacked analysis including systematics is the one with nuisance parameters and the covariance matrix.

| Pixel(s) | Pixel comb. | Run(s) | Run comb. | Uncertainty | $E_{0,\text{eff}}$ (eV) |
|----------|--------------|------------------|-----------|--------------|-------------------------|
| 0 | none | 40 667 | none | stat. only | $18\,576.8 \pm 3.0$ |
| all | uniform | 40 667 | none | stat. only | $18\,573.21 \pm 0.30$ |
| all | single-pixel | 40 667 | none | stat. only | $18\,573.11 \pm 0.27$ |
| all | multi-pixel | 40 667 | none | stat. only | $18\,573.20 \pm 0.32$ |
| 0 | none | 40 667 to 40 693 | appended | stat. only | $18\,574.40 \pm 0.62$ |
| all | uniform | 40 667 to 40 693 | stacked | stat. only | $18\,573.41 \pm 0.06$ |
| all | uniform | 40 667 to 40 693 | appended | stat. only | $18\,573.41 \pm 0.06$ |
| all | single-pixel | 40 667 to 40 693 | appended | stat. only | $18\,573.43 \pm 0.05$ |
| all | uniform | 40 667 to 40 693 | appended | stat. + sys. | $18\,574.19 \pm 0.20$ |
| all | uniform | 40 667 to 40 693 | stacked | stat. + sys. | $18\,574.33 \pm 0.24$ |

The statistical uncertainty when analysing a single run and a single pixel is 3.0 eV. When including a total of 121 pixels, the uncertainty drops to 0.27 eV to 0.32 eV corresponding to approximately a factor of 10. This is in good agreement with the statistical expectation of $\sqrt{121} = 11$. All three pixel combination methods agree within value and uncertainty. The analysis of a single pixel but 27 runs combined leads to an uncertainty around 0.62 eV. Compared to the single pixel, single run fit this is a decrease of about a factor of five which is again in agreement with the statistical expectation.

Stacking and appending runs leads to the same effective endpoint value and uncertainty. The uncertainty of 0.06 eV is also statistically expected in comparison with the uncertainty of a single pixel and single run, as: $\frac{3.0}{\sqrt{27 \cdot 121}} \approx 0.053$.

When adding systematic effects, the uncertainty of $E_{0,\text{eff}}$ is increased to 0.24 eV. All values for the effective endpoints are in good agreement with the expectation given the estimate of uncertainty on the work function difference of ± 0.5 eV as shown in figure 5.11.

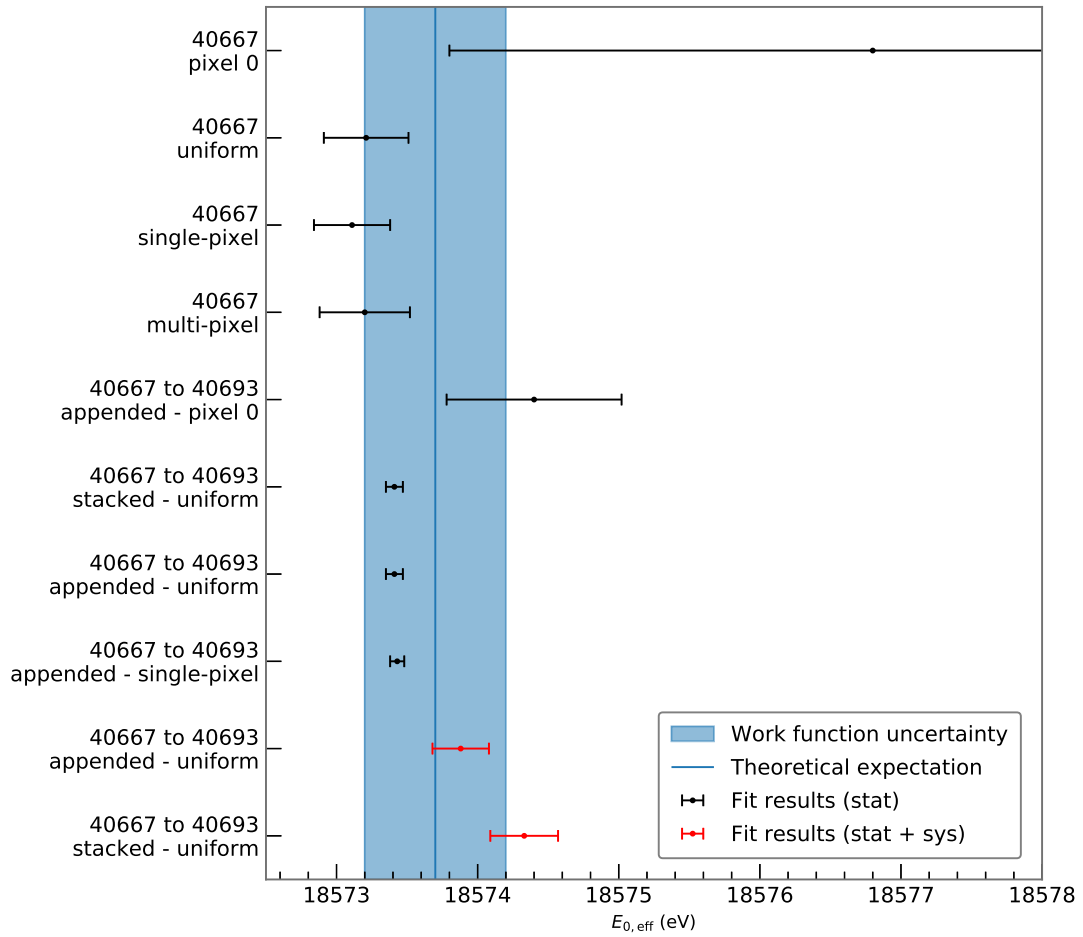


Figure 5.11: Overview of fit results from different analysis strategies. All results are in good agreement with the expectation. The appended analysis including systematics corresponds to the one in 5.4.3 with only nuisance parameters whereas the stacked analysis including systematics is the one with nuisance parameters and the covariance matrix.

Chapter 6

Conclusion and Outlook

In this thesis the first tritium data of the KATRIN experiment was analysed and based on this data set, different analysis strategies to combine data from different pixels and runs as well as systematics treatment were realized and successfully tested. To this end, a new analysis tool *Fitrium* was developed and employed.

Three different strategies for combining pixels, the *uniform*, *single-pixel* and *multi-pixel* fit, were worked out. With the sensitivity of first tritium data, all three are in good agreement. This statement will no longer hold for neutrino mass analysis as pixel-dependent effects matter at the increased statistics and the *uniform* fit is therefore no longer valid.

Concerning the combination of the spectra of different runs, two strategies were investigated: *run stacking* and *run appending*. While *stacking* eases data handling, *appending* makes no approximation. At the sensitivity of first tritium data, no significant difference was observed.

Finally, three different techniques to include systematic uncertainties were investigated: the *nuisance parameter*, *Monte Carlo propagation* and *covariance matrix* approach. The *nuisance parameter* method has proven to be feasible. Including multiple systematic effects in the analysis using this method led to an increase of uncertainty of the effective endpoint and improved the deviance distribution. Downside of this approach is the increase in fit complexity that comes with introducing more free parameters. The full Monte Carlo propagation was shown to lead to similar results, however, it is very computationally expensive and may not be the preferred path for the future. Also the analysis with the *covariance matrix* led to consistent results. This method is being investigated in detail with the so-called *SAMAK* analysis tool.

As a result of the analysis presented in this work, a good agreement between model and data could be demonstrated. The effective endpoint of the tritium spectrum is stable over time and distributed homogeneously over the KATRIN detector. Background values are stable from run to run but a clear radial and azimuthal dependence is visible. In a combined analysis including major systematic effects, the value of the effective endpoint is found to be $E_{0,\text{eff}} = 18574.33 \pm 0.24 \text{ eV}$. Taking into account the uncertainty on the work function difference between source and main spectrometer, this is in good agreement with the expectation.

The analysis tools and strategies developed in this thesis will serve as a basis for the forthcoming neutrino mass measurement. In the future with increasing statistical sensitivity the comparison of the different data combination methods will continue. As a next step, more effects such as synchrotron radiation and theoretical corrections will be included in the *Fitrium* model.

Further optimization of the fitting strategy will be required. An option here is to use a run-wise model or grouping runs depending on their slow control parameters. Systematic effects for first tritium are different than the ones in the upcoming neutrino mass measurement. Therefore these will have to be investigated with care. To treat them, the *nuisance parameter* and the *covariance matrix* approach can be utilized and combined.

Bibliography

- [1] C. L. Cowan Jr. et al. “Detection of the Free Neutrino: A Confirmation”. In: *Science* 124 (1956), pp. 103–104. DOI: [10.1126/science.124.3212.103](https://doi.org/10.1126/science.124.3212.103).
- [2] Y. Fukuda et al. “Evidence for Oscillation of Atmospheric Neutrinos”. In: *Phys. Rev. Lett.* 81 (8 1998), pp. 1562–1567. DOI: [10.1103/PhysRevLett.81.1562](https://doi.org/10.1103/PhysRevLett.81.1562). URL: <https://link.aps.org/doi/10.1103/PhysRevLett.81.1562>.
- [3] Q. R. Ahmad et al. “Direct Evidence for Neutrino Flavor Transformation from Neutral-Current Interactions in the Sudbury Neutrino Observatory”. In: *Phys. Rev. Lett.* 89 (1 2002), p. 011301. DOI: [10.1103/PhysRevLett.89.011301](https://doi.org/10.1103/PhysRevLett.89.011301). URL: <https://link.aps.org/doi/10.1103/PhysRevLett.89.011301>.
- [4] S. Abe et al. “Precision Measurement of Neutrino Oscillation Parameters with KamLAND”. In: *Phys. Rev. Lett.* 100 (22 2008), p. 221803. DOI: [10.1103/PhysRevLett.100.221803](https://doi.org/10.1103/PhysRevLett.100.221803). URL: <https://link.aps.org/doi/10.1103/PhysRevLett.100.221803>.
- [5] B. Pontecorvo. “Mesonium and anti-mesonium”. In: *Sov. Phys. JETP* 6 (1957). [Zh. Eksp. Teor. Fiz.33,549(1957)], p. 429.
- [6] Ziro Maki, Masami Nakagawa, and Shoichi Sakata. “Remarks on the Unified Model of Elementary Particles”. In: *Progress of Theoretical Physics* 28.5 (1962), pp. 870–880. DOI: [10.1143/PTP.28.870](https://doi.org/10.1143/PTP.28.870). eprint: [/oup/backfile/content_public/journal/ptp/28/5/10.1143/ptp.28.870/2/28-5-870.pdf](http://www.oup.com/backfile/content_public/journal/ptp/28/5/10.1143/ptp.28.870/2/28-5-870.pdf). URL: <http://dx.doi.org/10.1143/PTP.28.870>.
- [7] Steen Hannestad. “Neutrino physics from precision cosmology”. In: *Progress in Particle and Nuclear Physics* 65.2 (2010), pp. 185–208. ISSN: 0146-6410. DOI: <https://doi.org/10.1016/j.pnnp.2010.07.001>. URL: <http://www.sciencedirect.com/science/article/pii/S0146641010000499>.
- [8] Steven R. Elliott and Petr Vogel. “DOUBLE BETA DECAY”. In: *Annual Review of Nuclear and Particle Science* 52.1 (2002), pp. 115–151. DOI: [10.1146/annurev.nucl.52.050102.090641](https://doi.org/10.1146/annurev.nucl.52.050102.090641). URL: <https://doi.org/10.1146/annurev.nucl.52.050102.090641>.
- [9] Ch Kraus et al. “Final results from phase II of the Mainz neutrino mass search in tritium β decay”. In: *The European Physical Journal C - Particles and Fields* 40.4 (2005), pp. 447–468. ISSN: 1434-6052. DOI: [10.1140/epjc/s2005-02139-7](https://doi.org/10.1140/epjc/s2005-02139-7). URL: <https://doi.org/10.1140/epjc/s2005-02139-7>.

- [10] V. N. Aseev et al. “Upper limit on the electron antineutrino mass from the Troitsk experiment”. In: *Phys. Rev. D* 84 (11 2011), p. 112003. DOI: [10.1103/PhysRevD.84.112003](https://doi.org/10.1103/PhysRevD.84.112003). URL: <https://link.aps.org/doi/10.1103/PhysRevD.84.112003>.
- [11] KATRIN Collaboration and KATRIN Collaboration. *KATRIN design report 2004*. Tech. rep. 51.54.01; LK 01; Auch: NPI ASCR Rez EXP-01/2005; MS-KP-0501. Forschungszentrum, Karlsruhe, 2005. 245 pp.
- [12] M. Kleesiek et al. *β -Decay Spectrum, Response Function and Statistical Model for Neutrino Mass Measurements with the KATRIN Experiment*. 2018. eprint: [arXiv:1806.00369](https://arxiv.org/abs/1806.00369).
- [13] E W Otten and C Weinheimer. “Neutrino mass limit from tritium decay”. In: *Reports on Progress in Physics* 71.8 (2008), p. 086201. URL: <http://stacks.iop.org/0034-4885/71/i=8/a=086201>.
- [14] Susanne Mertens. “Study of Background Processes in the Electrostatic Spectrometers of the KATRIN Experiment”. PhD thesis. 2012.
- [15] Martin Slezák. “Monitoring of the energy scale in the KATRIN neutrino experiment”. PhD thesis. Charles University in Prague, 2015. URL: http://www.katrin.kit.edu/publikationen/phd-Martin_Slezak.pdf.
- [16] Martin Babutzka. “Design and development for the Rearsection of the KATRIN experiment”. PhD thesis. 2014.
- [17] Florian Heizmann, Hendrik Seitz-Moskaliuk, and KATRIN collaboration. “The Windowless Gaseous Tritium Source (WGTS) of the KATRIN experiment”. In: *Journal of Physics: Conference Series* 888.1 (2017), p. 012071. URL: <http://stacks.iop.org/1742-6596/888/i=1/a=012071>.
- [18] S. Lukić et al. “Measurement of the gas-flow reduction factor of the KATRIN DPS2-F differential pumping section”. In: *Vacuum* 86.8 (2012), pp. 1126–1133. ISSN: 0042-207X. DOI: <https://doi.org/10.1016/j.vacuum.2011.10.017>. URL: <http://www.sciencedirect.com/science/article/pii/S0042207X11003800>.
- [19] W. Gil et al. “The Cryogenic Pumping Section of the KATRIN Experiment”. In: *IEEE Transactions on Applied Superconductivity* 20.3 (2010), pp. 316–319. ISSN: 1051-8223. DOI: [10.1109/TASC.2009.2038581](https://doi.org/10.1109/TASC.2009.2038581).
- [20] J.F. Amsbaugh et al. “Focal-plane detector system for the KATRIN experiment”. In: *Nuclear Instruments and Methods in Physics Research Section A: Accelerators, Spectrometers, Detectors and Associated Equipment* 778 (2015), pp. 40–60. ISSN: 0168-9002. DOI: <https://doi.org/10.1016/j.nima.2014.12.116>. URL: <http://www.sciencedirect.com/science/article/pii/S0168900215000236>.
- [21] Alejandro Saenz, Svante Jonsell, and Piotr Froelich. “Improved Molecular Final-State Distribution of HeT⁺ for the β -Decay Process of T₂”. In: *Phys. Rev. Lett.* 84 (2 2000), pp. 242–245. DOI: [10.1103/PhysRevLett.84.242](https://doi.org/10.1103/PhysRevLett.84.242). URL: <https://link.aps.org/doi/10.1103/PhysRevLett.84.242>.

- [22] J. W. Liu. “Total Inelastic Cross Section for Collisions of H₂ with Fast Charged Particles”. In: *Phys. Rev. A* 7 (1 1973), pp. 103–109. DOI: [10.1103/PhysRevA.7.103](https://doi.org/10.1103/PhysRevA.7.103). URL: <https://link.aps.org/doi/10.1103/PhysRevA.7.103>.
- [23] VN. Aseev et al. “Energy loss of 18 keV electrons in gaseous T and quench condensed D films”. In: *The European Physical Journal D - Atomic, Molecular, Optical and Plasma Physics* 10.1 (2000), pp. 39–52. ISSN: 1434-6079. DOI: [10.1007/s100530050525](https://doi.org/10.1007/s100530050525). URL: <https://doi.org/10.1007/s100530050525>.
- [24] D. N. Abdurashitov et al. “Electron scattering on hydrogen and deuterium molecules at 14–25 keV by the “Troitsk nu-mass” experiment”. In: *Physics of Particles and Nuclei Letters* 14.6 (2017), pp. 892–899. ISSN: 1531-8567. DOI: [10.1134/S1547477117060024](https://doi.org/10.1134/S1547477117060024). URL: <https://doi.org/10.1134/S1547477117060024>.
- [25] V. Hannen et al. “Deconvolution of the energy loss function of the KATRIN experiment”. In: *Astroparticle Physics* 89 (2017), pp. 30–38. ISSN: 0927-6505. DOI: <https://doi.org/10.1016/j.astropartphys.2017.01.010>. URL: <http://www.sciencedirect.com/science/article/pii/S0927650517300348>.
- [26] *boost C++ libraries*. URL: <https://www.boost.org/>.
- [27] Natasha Doss et al. “Molecular effects in investigations of tritium molecule β decay endpoint experiments”. In: *Phys. Rev. C* 73 (2 2006), p. 025502. DOI: [10.1103/PhysRevC.73.025502](https://doi.org/10.1103/PhysRevC.73.025502). URL: <https://link.aps.org/doi/10.1103/PhysRevC.73.025502>.
- [28] The Free Software Foundation. *GNU Scientific Library*. URL: <https://www.gnu.org/software/gsl/>.
- [29] *Hierarchical Data Format*. URL: <https://www.hdfgroup.org/>.
- [30] R. Adhikari et al. “A White Paper on keV sterile neutrino Dark Matter”. In: *Journal of Cosmology and Astroparticle Physics* 2017.01 (2017), p. 025. URL: <http://stacks.iop.org/1475-7516/2017/i=01/a=025>.
- [31] Marco Kleesiek. “A Data-Analysis and Sensitivity-Optimization Framework for the KATRIN Experiment”. PhD thesis. 2014.
- [32] M. Arenz et al. “First transmission of electrons and ions through the KATRIN beamline”. In: *Journal of Instrumentation* 13.04 (2018), P04020. URL: <http://stacks.iop.org/1748-0221/13/i=04/a=P04020>.
- [33] Udo Schmitt. “Entwicklung eines Monitor-detektors für das KATRIN-Experiment”. German. PhD thesis. 2009.
- [34] Fabian Block. *Characterisation of the Background in the KATRIN Experiment*. 2018.
- [35] Thierry Lasserre, Pablo Morales, and Lisa Schlüter. *Simulation and Analysis of the First KATRIN Tritium Data with Samak*. 2018. URL: <https://neutrino.ikp.kit.edu/katrin/images/7/7f/Samakfirsttritium.pdf>.

Appendices

Appendix A

Slow Control Parameter Values for First Tritium Measurements

The values of the slow control parameters during KATRIN *very first tritium* (VFT) and *first tritium* (FT) measurements used for modelling are summarized here.

Table A.1: Slow control parameter values for VFT and FT.

| Parameter | VFT value | FT value |
|------------------------------|-------------------------------------|-------------------------------------|
| B_S | 2.52 T | 2.52 T |
| B_{\max} | 4.2 T | 4.2 T |
| B_{\min} | 6×10^{-4} T | 6×10^{-4} T |
| ρd | $4.5 \times 10^{21} \text{ m}^{-2}$ | $4.5 \times 10^{21} \text{ m}^{-2}$ |
| $\epsilon_{\text{detector}}$ | 95 % | 95 % |
| ϵ_{T_2} | 0.0 % | 0.0 % |
| ϵ_{HT} | 0.0 % | 0.0 % |
| ϵ_{DT} | 0.9 % to 1.2 % | 1.0 % |

Appendix B

Derivation of Relative Number of Counts in Endpoint Region

In the endpoint region $E \approx E_0$ the differential decay rate (2.5) neglecting the neutrino mass can be approximated by

$$\frac{d\Gamma}{dE} = C \cdot F(Z', E) \cdot p \cdot (E + m_e) \cdot (E_0 - E)^2 \quad (\text{B.1})$$

$$\approx C \cdot F \sqrt{(E_0 + m_e)^2 - m_e^2} \cdot (E_0 + m_e) \cdot (E_0 - E)^2 \quad (\text{B.2})$$

$$\propto E_0^2 \cdot (E_0 - E)^2 \quad (\text{B.3})$$

The number of counts in a small interval ΔE close to the endpoint is then

$$\Delta N \propto E_0^2 \int_{E_0 - \Delta E}^{E_0} (E_0 - E)^2 dE = E_0^2 \cdot \frac{1}{3} \Delta E^3 \quad (\text{B.4})$$

$$\propto E_0^2 \quad (\text{B.5})$$

while the total number of counts N is

$$N = \int_0^\infty \frac{d\Gamma}{dE} dE \propto E_0^5 \text{ }^1. \quad (\text{B.6})$$

Therefore the relative number of counts in the endpoint region is

$$\frac{\Delta N}{N} \propto \frac{1}{E_0^3}. \quad (\text{B.7})$$

¹Integral calculation is straightforward but tedious.

Appendix C

In-Depth Code Explanation of Fitrium

In this appendix an in-depth explanation of the ideas behind the C++ code of *Fitrium* is given.

Fitness Studio Base Classes

Fitrium, building upon the Fitness Studio, makes use of various base classes provided by it. The ones important for understanding the following code are briefly explained here.

ModelBase

This class is used as base class for every model, examples include the differential spectrum and the response function. `ModelBase` takes care of parameter handling and provides an interface for treating explicit derivatives (see 4.4) of these parameters.

The inherited class must mainly provide the `Evaluate` method which calculates the model value given the current parameter values and pass the parameters with explicit derivatives to `ModelBase` upon construction.

DataPointBase

`DataPointBase` is the simplest possible data point, a single value corresponding to the independent variable. Inherited classes can add to this information. For example, `DataPointPoisson` adds counts and times and `DataPointNormal` adds a dependent variable with an uncertainty. For the following code, it is sufficient to consider the data point as the value of the independent variable.

Model Decoupling

The different building blocks of the *Fitrium* model shown in figure 4.1 are loosely coupled classes that allow changing different parts without affecting the whole. How this works is explained in this section using two different examples.

Changing Signal or Background Model

As explained in 4.2, the basic building block is the description of a single pixel of the detector in `ModelPixel`. Its three components, signal, background and detector are passed to it in the constructor. Both the signal and the background must inherit from `ModelBase`.

```
// Pass signal, background and detector class in the constructor
ModelPixel(ModelBase &model, ModelBase &background, Detector detector);
```

The `ModelPixel` stores model, background and detector and knows how to combine the information from them to retrieve the rate expectation of the single pixel in its `Evaluate` method.

```
// Calculate rate expectation of single pixel
double ModelPixel::Evaluate(const DataPointBase &point) const
{
    return (fSignalModel.Evaluate(point) * fDetector.SignalPrefactor()
            + fBackgroundModel.Evaluate(point))
           * fDetector.Normalization();
}
```

As the only requirement to the signal and background model is to provide the `Evaluate` method, which is already needed by `ModelBase`, different model implementations can be passed as signal or background without implying changes to `ModelPixel`.

Changing Differential Spectrum or Response Function

Similar to `ModelPixel`, the integrated spectrum takes the differential spectrum and the response function by reference to their base class in the constructor.

```
// Pass differential spectrum and response function in the constructor
// ... substitutes additional parameters not required for understanding
IntegratedSpectrum(ModelBase &diffspec, ResponseBase &response, ...)
```

To use a different differential spectrum or response function one can pass these updated classes to the constructor as long as they inherit from the appropriate base class. The integrated spectrum can remain the same.

Building and Configuration

As parameter values and other settings are changed often, a flexible configuration and build structure has been developed to allow varying these options without having to touch the source code. All objects must be defined upon construction. The basic build process can be split into two parts:

1. Retrieve properties.
2. Construct objects.

This two-step process is reflected in the builder structure. A base class `BuilderBase` can construct the objects but it must be combined with another class which knows how to retrieve properties. These can be of different type, for example `BuilderIni` reads properties from the ini configuration file while `BuilderHDF5` reads in data files in the HDF5 format [29]. The base class is templated in the `BuilderType` and the corresponding builder is passed to the base class on construction. The object of type `BuilderType` must implement the `GetProperty` method for `BuilderBase`.

```
1  template <class BuilderType>
2  class BuilderBase
3  {
4  public:
5      // Initialize base class with builder of BuilderType.
6      BuilderBase(BuilderType builder);
7
8      // Dummy method to show builder principle.
9      Object CreateObject() const
10     {
11         return Object(fBuilder.GetProperty(BuilderKey::Property1));
12     }
13     ...
14 private:
15     // Templated builder class to retrieve properties from.
16     const BuilderType fBuilder;
17 };
```

As hinted in line 11, all properties are defined as objects of type `BuilderKey`. The `BuilderKey` stores type of the object (`double`, `bool`, `int`, ...), the path to this property in configuration file and data file as well as a default value to fall back to. This ensures a unified structure of the `GetProperty` method and provides for adding new properties by creating a new `BuilderKey` object with the appropriate three arguments.

```
template <typename OptionType>
struct BuilderKey {
    BuilderKey(std::string ini_path, std::string hdf5_path,
              OptionType default_value)
        : IniPath(ini_path), HDF5Path(hdf5_path), DefaultValue(default_value)
    {
    }

    const std::string IniPath; // Path in configuration file
    const std::string HDF5Path; // Path in data file
    const OptionType DefaultValue; // Fallback default value
};
```

What is left for the templated builder is then to define the `GetProperty` method. This is shown here for the `BuilderIni` which reads the configuration file.

```
class BuilderIni
{
public:
    // Read ini file on construction.
    BuilderIni(std::string filename);

    // Retrieve a property from the ini file.
    template <class OptionType>
    inline OptionType GetProperty(BuilderKey::BuilderKey<OptionType> key) const
    {
        return fPropertyTree.get(key.IniPath, key.DefaultValue);
    }
    ...
private:
    // Tree storing all the options read from the ini file.
    boost::property_tree::ptree fPropertyTree;
};
```

The structure of the ini file which is read is shown below.

[Detector]

```
; Efficiency of the detector
Efficiency = 0.9
; Number of pixels the detector is divided in
NPixels = 148
; Pixels used for the analysis
;
; Pixels are indexed from 0. The largest number must therefore be smaller than
; (NPixels - 1). Pixels not listed here are excluded from the analysis. It is
; possible to define ranges, e.g. 0-147 and comma separated values, e.g. 1,2.
; Combining both is possible. '*' means activate all pixels.
;
; Full example: ActivePixels = 0-120,122,123
ActivePixels = *
```

Appendix D

Monte Carlo Generator for KATRIN

At the beginning of the work on this thesis, a Monte Carlo (MC) generator for the KATRIN experiment was developed. A MC generator produces artificial data sets that look like the real ones by simulating the model theoretically and applying statistical smearing. The use cases for such a tool include testing the fitting tools and investigating the effect of various systematics on the neutrino mass measurement.

An overview of the working principle is shown in figure [D.1](#). The theoretical model used by the MC generator is *SSC* (Source and Spectrum Calculation) [[31](#), p. 85]. Configuration of model and other parameters is done using an initialization file very similar to the one of *Fitrium*.

First, the so called “run plan”, must be defined. It contains information describing how much measuring time is spent at which retarding potential. The model now calculates the expected rate for each retarding energy and multiplies it with the measuring time. This average number of counts is fluctuated randomly using a Poisson distribution to retrieve the Monte Carlo data set. The data set is then written to a *run summary* file which can be converted to HDF5 for *Fitrium*.

The developed MC generator was successfully used for testing fitting tools, not only *Fitrium*. Most of the functionality has been merged with the *Fitrium* package where the underlying model is no longer *SSC*.

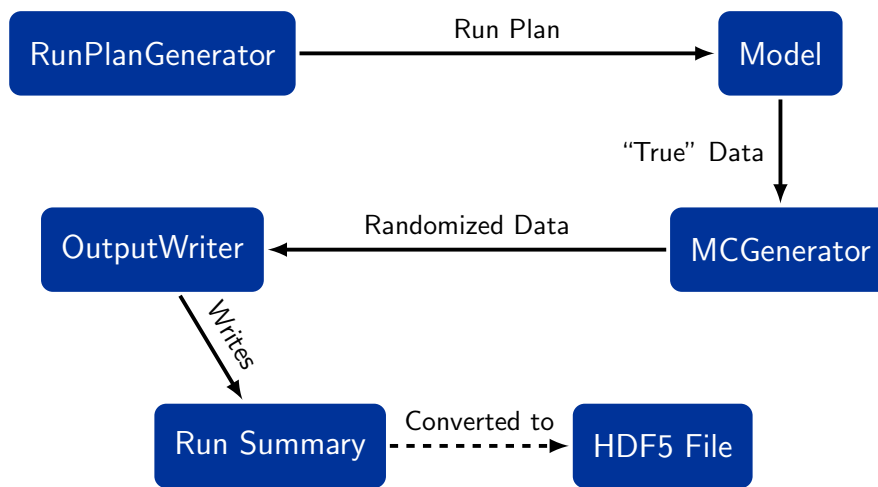


Figure D.1: Structure of the MC Generator. A run plan is passed to the model which calculates the average counts for every retarding energy. This data is fluctuated and the retrieved counts with all the other information is written to the run summary. It is possible to convert the run summary to the HDF5 format.

Appendix E

Additional Figures

Here additional figures that are not required for the understanding of the thesis but illustrate the capabilities of the plotting tool *Plotrium* are displayed.

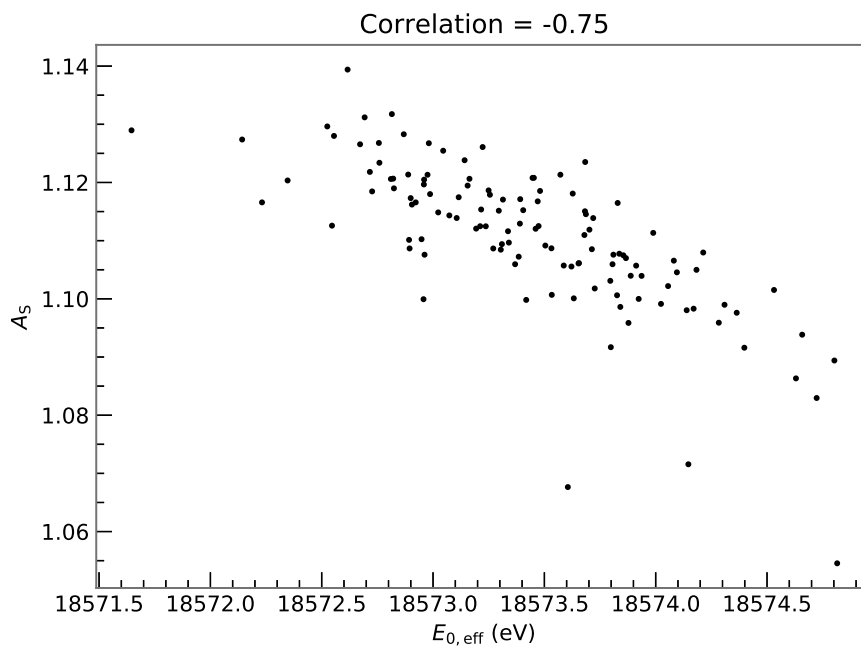


Figure E.1: Correlation of effective endpoint and normalization. The points correspond to the fit result of single pixel fits of runs 40 667 to 40 693 appended, statistical uncertainty only. The correlation of -0.75 is Pearson's correlation coefficient.

Acknowledgements

I would like to thank everyone who helped me during my Master's thesis, in particular:

- Prof. Dr. Susanne Mertens for giving me the chance to work on this thesis and her incredible supervision with lots of fruitful discussions and permanent support,
- Dr. Martin Slezák for his constant support concerning coding, physics and more and for developing the *Fitness Studio*,
- Dr. Sanshiro Enomoto for all his work on KATRIN software, in particular for his permanent efforts in creating and improving the *run summary* files,
- Frank Edzards for the great atmosphere in our shared office and lots of rewarding discussions at the beginning of *Fitrium* development,
- all PhD, fellow Master's and other students in the TRISTAN group at MPP for a great time and support on various topics,
- the KATRIN collaboration for the warm welcome and the opportunity to work on KATRIN,
- the free software community for helping me improve my coding skills and providing an innumerable amount of great tools,

and of course my family, girlfriend and friends for their permanent encouragement making this thesis possible at all.